Influence of STM measurements on vacancies physics in graphene

Yuval Abulafia

Influence of STM measurements on vacancies physics in graphene

Research Thesis

Submitted in partial fulfillment of the requirements
for the degree of Master of Science in Physics

Yuval Abulafia

Submitted to the Senate
of the Technion — Israel Institute of Technology
Tishre 5781 Haifa September 2020

This research was carried out under the supervision of Prof. Eric Akkermans, in the Faculty of Physics.

Acknowledgements

I would like to sincerely thank my advisor Prof. Eric Akkermans for his guidance and support during the entire research and especially while writing this thesis. Each conversation was fruitful and educative, you helped me to organize my ideas, understand how to approach a problem and your comments led to new thoughts and approaches regarding the research. For this I am truly thankful.

A special acknowledgement for my parents and family for supporting and inspiring me throughout my entire life.

The generous financial help of the Technion is gratefully acknowledged.

Contents

List of Figures

Abstract

Graphene, a two dimensional honeycomb lattice, is a fascinating material that gathers researchers from a wide variety of fields. Physicists, are interested in its transport and thermodynamic properties and the relation to massless fermion field. One of the experimental recent goals was to achieve a stable local charge in graphene, a non trivial task given its high conductivity. A successful method though was found, creating vacancies - a removal of neutral carbon atoms from the lattice.

In addition to local stable charge, the creation of vacancies leads to two more intriguing physical features. First, the breaking of parity symmetry was confirmed both theoretically and experimentally and second, additional zero energy modes show up in the spectrum. Since no additional energy scale was added by the creation of vacancies, theoretically we would expect these zero energy modes to be exactly at the Fermi energy. Yet, experimentally these modes deviates from zero by a sizeable amount.

This deviation is particularly interesting due to graphene symmetric energy spectrum, whose origin is in the bipartite nature of the lattice. i.e. the partition of the lattices sites into two groups. Each site in every group should interact only with sites of the other group. Therefore, neglecting next nearest neighbors interaction means that graphene lattice is bipartite and it is easy to show that its spectrum should be symmetric. The shift in the location of the "zero energy modes" breaks the symmetry of the spectrum and has not been explained so far.

In our work, we show that this shift can be related, at least partly, to the interaction with the measurement device - scanning tunnelling microscopy (STM). This measurement device consists of electrons tunnelling between the sample and the STM tip, which create a current that is measured and analysed. We take into consideration both the Hamiltonian of graphene with a vacancy, the STM system and the tunneling interaction term between them. Next, we estimate and analyse the contribution of each separate part of the Hamiltonian. Furthermore, we point out an important step in the calculation which is usually neglected.

Finally, we attempt to solve (left for future work) the problem of high voltage pulses

which change the accumulated stable charge on the vacancy boundary. This problem has a time dependent Hamiltonian. Thus, we propose a mapping that might relate the problem of vacancy to a gauge field. This mapping can simplify the problem while preserving all physical properties of the system.

Abbreviations and Notations

STM	:	Scanning tunneling microscope
STS	:	Scanning tunneling spectroscopy
LDOD	:	Local density of states
QED	:	Quantum electrodynamics
a.u	:	Arbitrary units
ZM	:	Zero mode

Chapter 1

Introduction

This chapter is divided into two parts, the first part presents the main question we have addressed and results we have obtained without entering into the details. The second part of the introduction is devoted to exposing the main properties of graphene which are of interest to us in this work. Namely, the Hamiltonian in the coarse-grained limit, two ways to model vacancies, either using a Coulomb potential or specifically tailoring chiral boundary conditions.

Graphene a single layer honeycomb lattice of carbon atoms, is a two dimensional material which triggered major interest (in physics, chemistry and material science) from the very beginning [1] due to its numerous properties, ranging from electronic properties [2] to unusual optical behavior [3, 4], mechanical strength [5], high thermal conductivity [6], etc.. In addition to these features, it is admitted that graphene can be represented at low temperature by a massless non interacting Dirac fermion field [7]. This description is useful to model more complex problems, such as graphene with impurities or defects [8–10], representing graphene itself by a massless Dirac fermion field and defects using their physical characteristics. One type of defect is a vacancy, obtained by the removal of a neutral carbon atom from the lattice.

The physics of vacancies in graphene is rich and interesting due to the appearance of many surprising features that we now briefly review. Measurement data show that the resistivity behavior is according to the Kondo effect [11] and that localized electronic states build up near the vacancy sites (see Figure 1.1 left) [12]. Both provide a strong evidence of magnetic order at the vacancies. In addition, the wave function of spatially localized modes match the potential calculation of a charge state [13], therefore suggesting charge accumulation around the vacancy boundaries. Furthermore, a zero energy mode shows up in the energy spectrum (see Figure 1.1 right) [12, 14] together with measurements that confirm parity symmetry breaking predicted theoretically [15]. Finally, the application of high voltage pulses via scanning tunneling microscopy (STM) tip changes the stable charge that accumulated around the vacancy [14, 15].

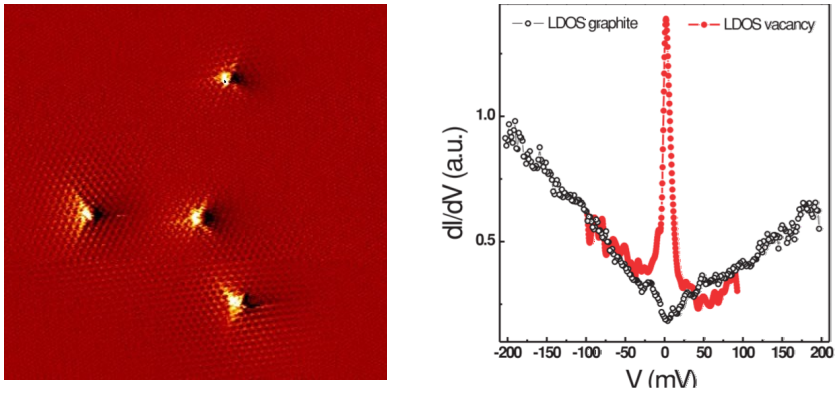

Figure 1.1: Measurement of [12]. (Left) scanning tunneling microscope (STM) measurements of (17×17) nm^2 graphite sample after Ar^+ ion irradiation. (Right) local density of states (LDOS) scanning tunneling spectroscopy (STS) measurement without (black) and with (red) vacancy.

Although it seems that the location of the additional energy mode is exactly at the Fermi energy (zero) (see Figure 1.1 right), this is not the case. A closer look emphasises that this zero energy mode is shifted from the Fermi energy (see Figure 1.2). So far the theory did not explaind this deviation.

In this work we propose a theoretical explanation for the shift of the zero energy mode. Our approach is via the interaction with the measurement apparatus (STM) such that the full Hamiltonian is:

$$H = H_{graphene} + T + H_{STM}, \tag{1.1}$$

where $H_{graphene}$ (H_{STM}) are respectively the Hamiltonians of isolated graphene with a vacancy (the STM) and T is the interaction term between them. In the STS apparatus the tunneling conductance $\frac{dI}{dV}$ is measured (tunneling current with respect to the voltage difference between the STM and the sample), therefore in our work the tunneling conductance has been evaluated. We wish to stress that our calculation is more involved than the standard 'text-book' approach. Comparison between the two tunneling conductance expressions (our and the standard Fermi golden rule) is detailed in future chapters. However, let us first sketch the differences between them. Our expression for $\tilde{\sigma}(E) = \frac{dI}{dV}$, is

$$\tilde{\sigma}(E) \propto -\frac{e^2}{h} \frac{t^2 N_{STM}(E)\, N_G(E)}{\left| \left(I - t\, G_G^+(E)\, G_{STM,0}^+(E) \right) \right|^2}\ , \tag{1.2}$$

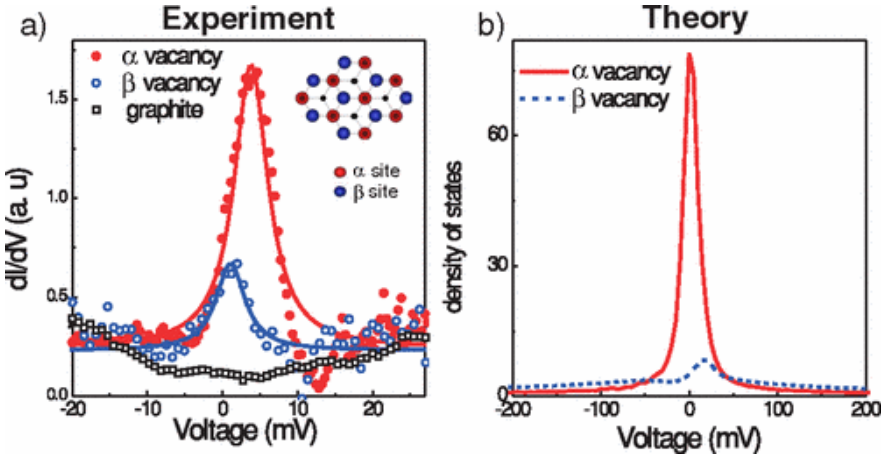

Figure 1.2: (Left) a different scale of STS graphene with vacancies measurement. It is clear that the additional zero mode slightly deviates from zero. The theory (right) does not explain this deviation [12].

as compared to the 'text book' Fermi golden rule expression (namely only the numerator):

$$\frac{dI}{dV} = 2\pi \frac{e^2}{\hbar} |t|^2 N_{STM} N_{sample} \ , \tag{1.3}$$

where t is the tunneling amplitude, N_G (N_{STM}) is the local density of states of graphene (STM) and G_G (G_{STM}) is the Green's function of the isolated graphene (STM). The full expression is derived in the next chapter.

Our first goal is to evaluate this expression and compare with the measured data, in order to explain the shifted zero energy mode. Next, we further analyze our numerical solution and the contribution of each term of our expression to the tunneling conductance, so as to answer the question of whether our involved formula is needed rather than a simpler expression. However, for now we only display our results - that the tunneling interaction partly explains this zero mode shift (see Figure 1.3).

At the end of our work, we try to explain the basic physics behind the charge accumulation. As for now, models of graphene with vacancy manage to predict the charge accumulation [16] but do not predict the behavior under STM high voltage pulses (time dependent potential). We hope to explain this behavior using a mapping to a different system with the same physical properties but without a vacancy.

To further explain our approach let us elaborate on the behavior of graphene with vacancies.

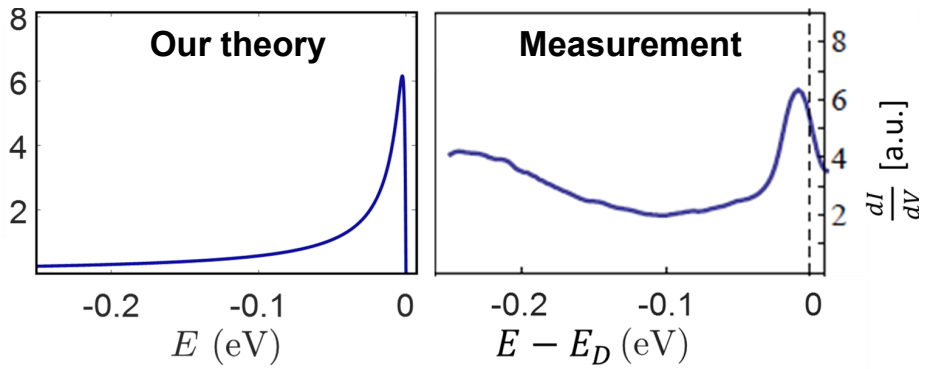

Figure 1.3: Tunneling conductance results; experiment vs. theory. (Left) our model taking into account the interaction with the STM via tunneling term in the Hamiltonian. (Right) experimental data [15]. Comparing the zero mode shifts gives 2.3meV in our calculations v.s. 8.3meV in the measurements.

1.1 Graphene: Basic properties

The graphene lattice is a superposition of two triangular sublattices (see Figure 1.4). The Hamiltonian of graphene in the tight binding approximation:

$$\mathcal{H} = -\sum_{\boldsymbol{R}\in\Lambda_A}\sum_{i=1}^{3} t\, a^{\dagger}_{\boldsymbol{R}} b_{\boldsymbol{R}+\boldsymbol{s}_i} + h.c\ , \tag{1.4}$$

where Λ_A represents the sites of sublattice A, $\mathbf{R}$ belongs to Λ_A, $a_{\boldsymbol{R}}$ ($b_{\boldsymbol{R}}$) destroys electron located at $\boldsymbol{R}$ from sublattice A (B) and $a^{\dagger}_{\boldsymbol{R}}$ ($b^{\dagger}_{\boldsymbol{R}}$) creates electron located at $\boldsymbol{R}$ from sublattice A (B). $\boldsymbol{s}_i$ connects an atom to its nearest neighbors and t is the energy hopping from one atom to its nearest neighbors. The corresponding energy spectrum exhibits two Dirac points [17].

The Hamiltonian, as written in (1.4), assumes that graphene is a bipartite lattice, namely the two sublattices interact only through sites from the other sublattice (there is no direct connection between atoms on the same sublattice). Considering the next nearest term - t', breaks this symmetry since it connects atoms from the same sublattice. However, according to numerical fit done by [18] $t = 2.97$eV, $t' = 0.073$eV and $t'' = 0.33$eV. Thus, since t' is small in comparison to t the assumption of a bipartite lattice seems justified.

1.1.1 Behavior near Dirac points

Solving the tight binding model for graphene, one notices that the graphene spectrum has two distinguished Dirac points (see Figure 1.5). Around these points low energy excitations can be linearized. Moreover, the two atoms in the graphene unit cell form a

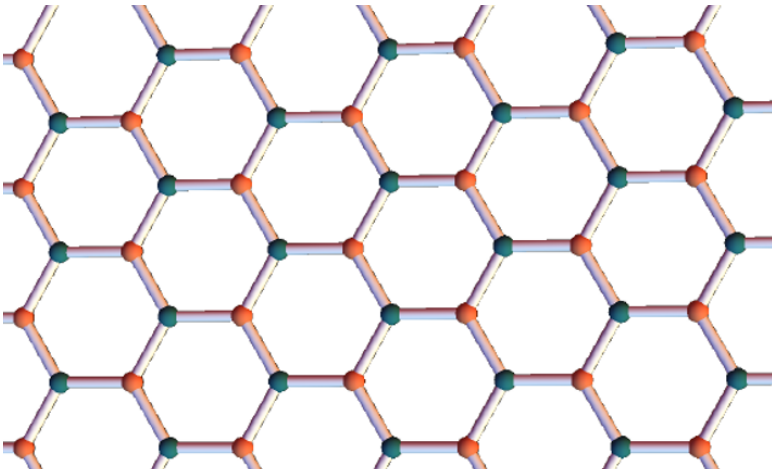

Figure 1.4: Graphene honeycomb lattice of carbon atoms splitted into two triangular sublattices A and B (in red and blue)

spinor,

$$\psi = \begin{pmatrix} \psi_A \\ \psi_B \end{pmatrix} \ . \tag{1.5}$$

These specific features of graphene allow to map the graphene Hamiltonain using massless non-interacting Dirac field Hamiltonian [7],

$$\mathcal{H} = -i\boldsymbol{\sigma} \cdot \boldsymbol{\nabla} \ , \tag{1.6}$$

where σ is a vector of Pauli matrices and the Hamiltonian is written in units such that $v_F = 1$. This description holds in the continuum limit (lattice constant goes to zero) with low energy excitations.

As mentioned briefly earlier, graphene triggered interest in other fields such as high energy physics. This interest origins in the representation of graphene using a massless Dirac fermion field, which can interact with a vector field and accounts for 2+1 (two space dimensions and one time) quantum electrodynamics (QED).
The Lagrangian of 2+1 QED can be written as:

$$\mathcal{L} = \overline{\psi}(x)(i\gamma^\mu D_\mu - m)\psi(x) \ , \tag{1.7}$$

where $\psi(x)$ is a spinor field that represents a fermion with mass m coupled to a gauge field A_μ using covariant coupling $D_\mu = \partial_\mu - ieA_\mu$ and γ^μ satisfy the Clifford algebra $\{\gamma^\mu, \gamma^\nu\} = 2\eta^{\mu\nu}$. Since in our case the fermions are massless, then $m = 0$. (We will not elaborate any longer on that subject, postponing it to Chapter 3).

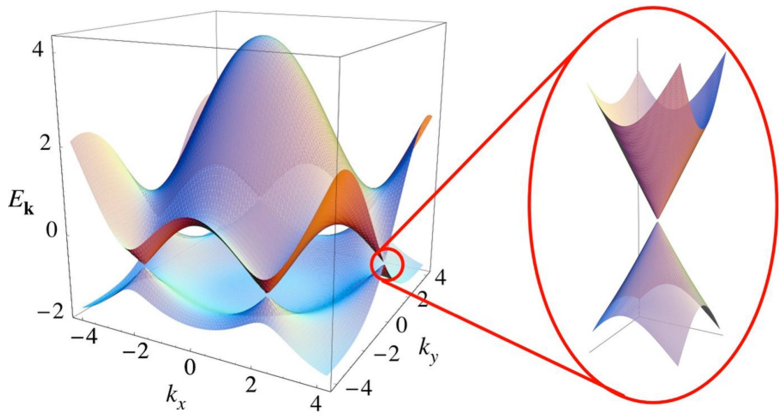

Figure 1.5: (Left) graphene energy spectrum from the tight binding model. (Right) a zoom into one of the Dirac points where the dispersion relation is linear [2].

1.1.2 Symmetries

Graphene symmetries and their physical impact enables us to understand important properties of graphene and when they should be broken. There are two important symmetries:

1. Symmetric energy spectrum - the Hamiltonian (1.6) anti-commutes with σ_3, given by

$$\sigma_3 = \begin{pmatrix} 1 & 0 \\ 0 & -1 \end{pmatrix} \tag{1.8}$$

This leads to a symmetric spectrum around $E = 0$ (see Figure 1.6).

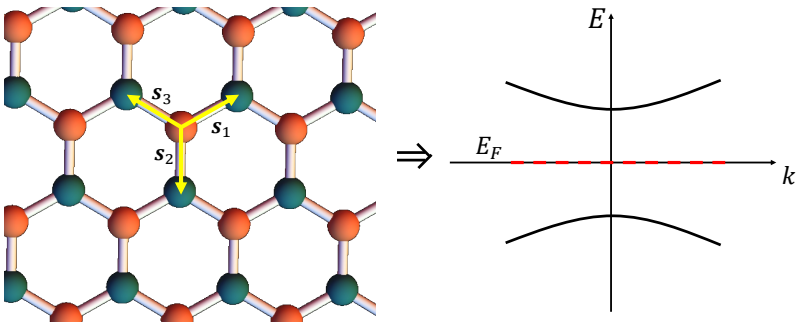

Figure 1.6: The spectrum is symmetric as a result of the bipartite nature of graphene lattice.

This symmetry results from the approximation that graphene is a bipartite lattice [19] and should be conserved as long as this is the case. We now show a simple proof for the symmetric spectrum [20, 21]:

Every Hamiltonian is described in some Hilbert space, which can always be separated into two subspaces. After doing so, all types of interactions can be sorted into interactions inside each subspace and between the two subspaces. Therefore, the Hamiltonian (1.6) can be written under this form:

$$\mathcal{H} = \begin{pmatrix} \Lambda_A \text{ with } \Lambda_A & \Lambda_A \text{ with } \Lambda_B \\ \Lambda_B \text{ with } \Lambda_A & \Lambda_B \text{ with } \Lambda_B \end{pmatrix} ,$$

where Λ_A (Λ_B) are sites from sublattice A (B). In the case of bipartite lattice, each site interacts only with sites from the other sublattice. Thus, no interactions within sublattice A or B are allowed. Therefore, the Hamiltonian can be written as:

$$\mathcal{H} = \begin{pmatrix} 0 & \hat{t} \\ \hat{t}^\dagger & 0 \end{pmatrix} , \tag{1.9}$$

in this form, it is clear that the Hamiltonian anti-commutes with σ_3,

$$\{\mathcal{H}, \sigma_3\} = 0 \ . \tag{1.10}$$

Furthermore, for each eigenstate $|\psi>$ of energy E,

$$\mathcal{H}|\psi>= E|\psi> \tag{1.11}$$

there is also a state $|\psi'>= \sigma_3|\psi>$ with opposite sign energy $-E$

$$\sigma_3\mathcal{H}|\psi>= E\sigma_3|\psi> \ , \tag{1.12}$$

$$\mathcal{H}|\psi'>= -E|\psi'> \ . \tag{1.13}$$

2. Parity - the lattice remains unchanged if one takes (see Figure 1.7):

$$\begin{cases} x \to x \\ y \to -y \\ \text{Sublattice } A\,(B) \to B\,(A) \end{cases} . \tag{1.14}$$

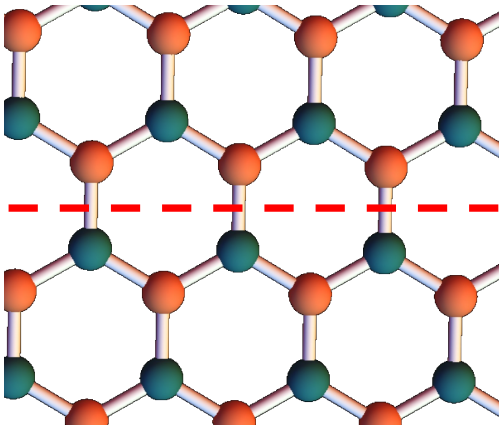

Figure 1.7: Parity symmetry - reflection of the system around the dashed red line and exchanging the two sublattices.

These two symmetries can be altered by the presence of vacancies in graphene.

1.2 Vacancies

A vacancy, is defined by the removal of a single neutral atom from the lattice (see Figure 1.8). Experimental works on graphene studied the formation of vacancies [22] and the lattice behavior with vacancies [13]. In addition to physical features mentioned above (and elaborated here), evidence of local magnetic moments was shown [12]. Moreover, recent approaches predict a charge fractionalization [16] on the boundary of a vacancy.

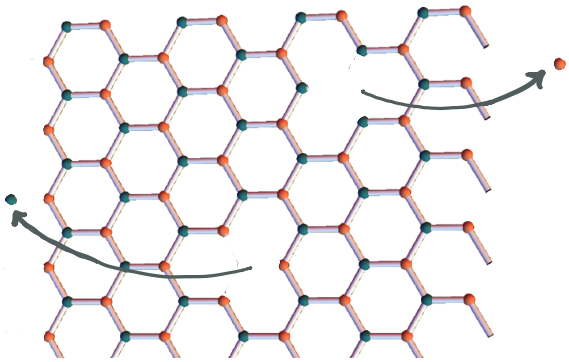

Figure 1.8: Creating vacancies by removing neutral atoms from the lattice, simply leads to bonds destruction.

The creation of vacancies breaks parity symmetry (see Figure 1.9). However, the σ_3 symmetry still holds, thus we expect the additional energy mode to be located exactly at zero (Fermi energy) (otherwise the spectrum is not symmetric around the Fermi energy).

Since the creation of a vacancy does not involve any new energy scale for the problem nor breaks the bipartite property, it should not lead to the breaking of this symmetry. Therefore, the measured small shift of this mode is caused by something else that breaks the σ_3 symmetry.

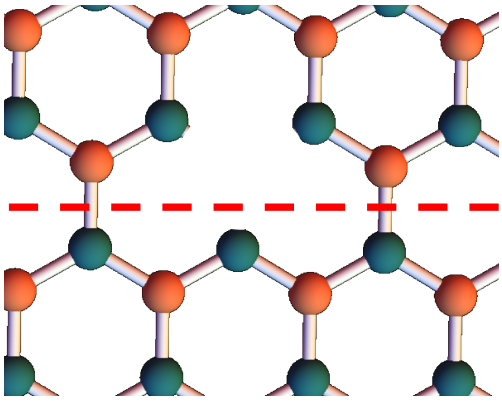

Figure 1.9: Breaking of parity symmetry, reflection and sublattice exchange no longer leaves the system unchanged.

The additional energy scale may result from the measurement apparatus. Since STM measurement is based on tunneling electrons, an interaction term with additional energy scale is introduced. Therefore, this term can explain the σ_3 symmetry breaking and the shifted zero mode.

The understanding of our approach to this problem requires a more thorough explanation about both the physical features of graphene with vacancies and currently available models.

As mentioned before, vacancies in graphene lead to interesting features:

1. Zero energy modes
2. Charge accumulation at the vacancy boundary
3. Breaking of parity symmetry

So far, both a solution using the tight binding model [23] (for a single vacancy), and two models that describes graphene with vacancies are available. The first approach was originally studied in order to characterize graphene with an unscreened charged impurity [8, 9, 24]. Therefore, it involves the addition of Coulomb term to the Dirac Hamiltonian:

$$H = -i\boldsymbol{\sigma} \cdot \boldsymbol{\nabla} - \frac{\beta}{r} \ , \tag{1.15}$$

where $\beta = Z\alpha$, Z is the Coulomb charge and α is the fine structure constant for graphene. Since $\alpha = \frac{1}{4\pi\epsilon_0}\frac{e^2}{\hbar c} \to \frac{1}{4\pi\epsilon_g}\frac{e^2}{\hbar v_F}$ (the speed of light c is replaced with $v_F \equiv \frac{3}{2}ta$, a is graphene lattice constant), α is much larger in graphene $\alpha_g \sim 1$ [2] instead of the known value $\alpha = 1/137$. Nevertheless, note that the dielectric constant ϵ_g in graphene is not known precisely.

This model though provides results that are in good agreement with the measurements of graphene with vacancies (see Figure 1.10) [15]. Since there are evidence of charge accumulation at the vacancy boundary, it is reasonable that it can be described using an unscreened Coulomb potential. However, this model has some disadvantages, mostly the fact that it can not predict β (proportional to the accumulated charge), whose values result from a fit of the data.

An additional surprising measurement result (see Figure 1.10) is the changing value of β in the experiment. Since β is proportional to the accumulated stable charge, we can infer that altering β means different stable charge state. This variation of the accumulated charge was achieved in the experiment [14] using high voltage pulses applied via the STM tip. The STM tip is spatially located above an isolated vacancy. Usually, STS measurements are preformed with some voltage difference, however in the case of pulses, the voltage applied from the tip is larger by two orders of magnitude than the regular measurement (both voltages are smaller than the tunneling potential barrier). This unexpected phenomena has not been explained yet. In the sequel, we consider a fixed value for the local charge.

The second approach [16], describes vacancy in graphene as a perfect scatterer. This description uses the Dirac Hamiltonian with specific boundary conditions called "chiral". This choice of boundary conditions, imposes a vanishing entrance of the probability density inside the vacancy radius, so that the vacancy behaves like a perfect scatterer. The description of graphene uses the Dirac Hamiltonian,

$$H = -i\boldsymbol{\sigma}\cdot\boldsymbol{\nabla}\ , \tag{1.16}$$

and the boundary conditions discriminate between the spectral modes of the two sublattices A and B where the integer m is the projection of the angular momentum:

$$\psi_m^A\left(r=R\right)=0, \qquad m\leq 0, \tag{1.17}$$

$$\psi_m^B\left(r=R\right)=0, \qquad m>0, \tag{1.18}$$

with the spectral decomposition:

$$\psi\left(r,\theta\right)\equiv\sum_{m\in\mathbb{Z}}e^{im\theta}\begin{pmatrix}\psi_m^A\left(r\right)\\ i\psi_m^B\left(r\right)e^{i\theta}\end{pmatrix}\ . \tag{1.19}$$

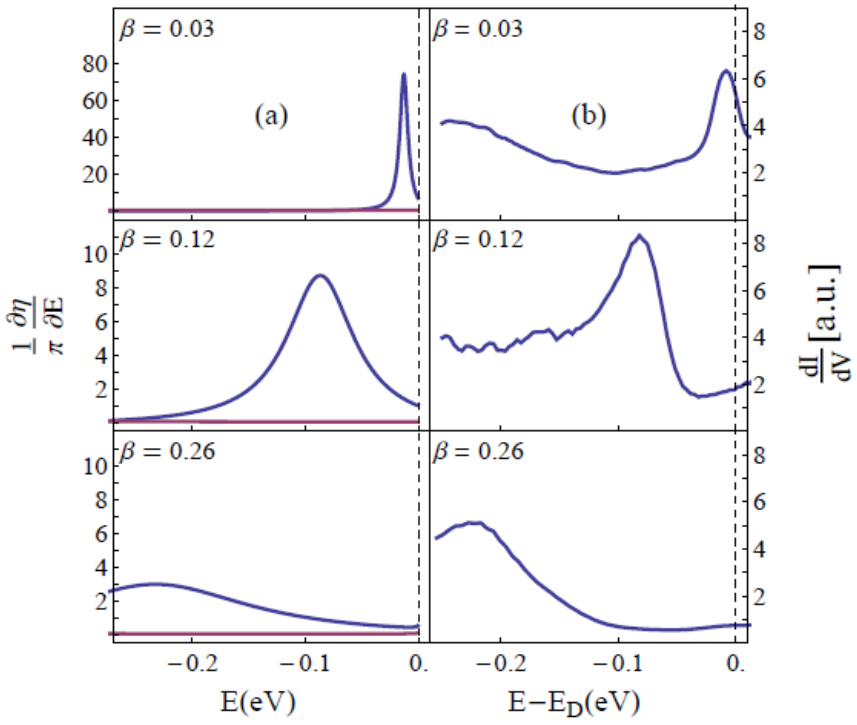

Figure 1.10: Charge built due to high voltage pulses, (right) experiment v.s. (left) theoretical results [15]. One can notice the small deviation of the peak for $\beta = 0.03$ from the exact zero.

This model manages to explain all three features of graphene with vacancies:

1. A zero energy mode appears in the spectrum. The removal of N_a (N_b) atoms from sublattice A (B) results in the appearance of $|N_a - N_b|$ additional zero energy modes. For further explanation via linear algebra see [25]. These zero energy modes have been measured (see Figure 1.1 right) [12] and indeed, show up in the spectrum, although their location slightly deviates from the Fermi energy (see Figure 1.2).

2. Even though a neutral atom was removed, charge accumulates at the boundary of the vacancy [14]. The creation of a vacancy causes a rearrangement of the electronic structure and results in spatially localized electronic wave function [13] (see Figure 1.1 left). Moreover, this model [16] predicts the charge density around a single vacancy and in the case of multiple vacancies, the total charge is:

$$Q = \frac{e}{2} |N_A - N_B| \quad . \tag{1.20}$$

3. Breaking of parity symmetry is achieved using chiral boundary conditions. This specific choice of boundary conditions discriminates between the two sublattices [16], so as to break parity symmetry.

According to the first approach (see Figure 1.10), it seems that the shifted energy mode is already explained. However, the obtained shifted energy mode is quite obvious, since it is caused directly from the β fit the theory is based on. Thus, the theory does not explain the fundamental physics behind this shift. Moreover, the description of graphene with vacancy using Coulomb potential does not fit properly the measured potential behavior.

In this work, the additional energy scale that breaks the σ_3 symmetry is suggested to be the interaction with the measurement STM apparatus. This interaction term has an energy scale, which is explained in details and calculated in the next chapters. In addition, there is no reason for the interaction with the STM to keep the σ_3 symmetry, therefore it can explain the small shift in the zero mode energy. Our choice for the description of graphene with vacancy is via the second model, using chiral boundary conditions. Equipped with it, we managed to explain the shifted zero energy mode without including an artificial Coulomb term to the Hamiltonian (as done in the first approach).

Finally, at the end of this work, the first step to the solution of the accumulated charge problem is introduced. Our main intention regarding this problem is to simplify the system of graphene with vacancies, which is explained using artificial boundary conditions. This suggested simplification is based on a mapping to a problem that replaces these boundary conditions by a gauge field. Further explanations about this mapping is proposed in Chapter 3.

Chapter 2

Tunneling Interaction

2.1 Scanning Tunneling Microscope - STM

STM is a measurement device based on electrons tunneling from the STM tip to the sample and vice versa. Its invention [26, 27] and the invention of STS - Scanning Tunneling Spectroscopy enhanced the spatial resolution to the order of atomic scale [14, 28, 29].

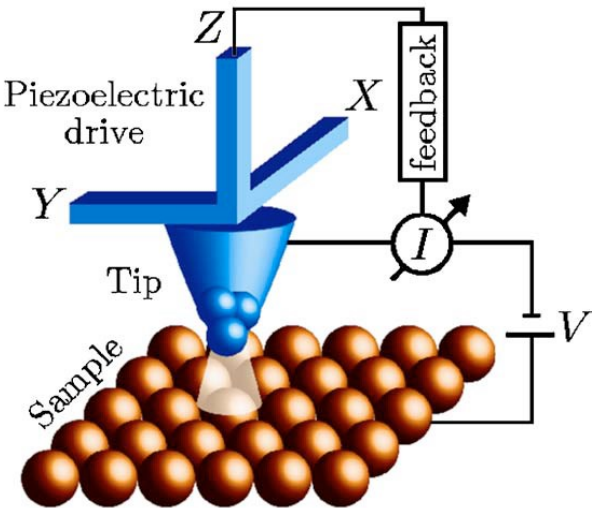

Figure 2.1: Simplified setup of STM measurement apparatus, tunneling current from the STM tip to the sample is monitored and the xy surface is scanned using piezoelectric drive. [29]

Tunneling current is highly sensitive to the distance between the STM tip and the sample (exponential decay with the distance) (see Figure 2.2) which enables high resolution topographic mapping of the sample surface. There are two measuring configurations of the STM (see Figure 2.3). The first one is with a constant current, the current is constantly monitored and when changed, the z piezoelectric drive along the z direction

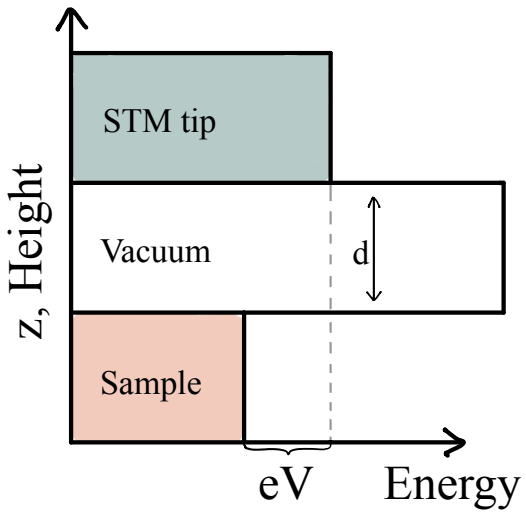

Figure 2.2: Electrons tunnel from the tip through a potential barrier of length d - the distance between the tip and the sample [29].

adapts the height of the tip such that the current retains its previous value and remains constant (see Figure 2.3 a). In this configuration the distance (z coordinate) is measured. In the second configuration, the height is constant and the current is measured (see Figure 2.3 b). When preforming a STS measurement, the STM tip is located above a spatially constant point and the applied voltage difference V varies, thus enabling the measurements of the current dependence in the voltage $\frac{dI}{dV}$.

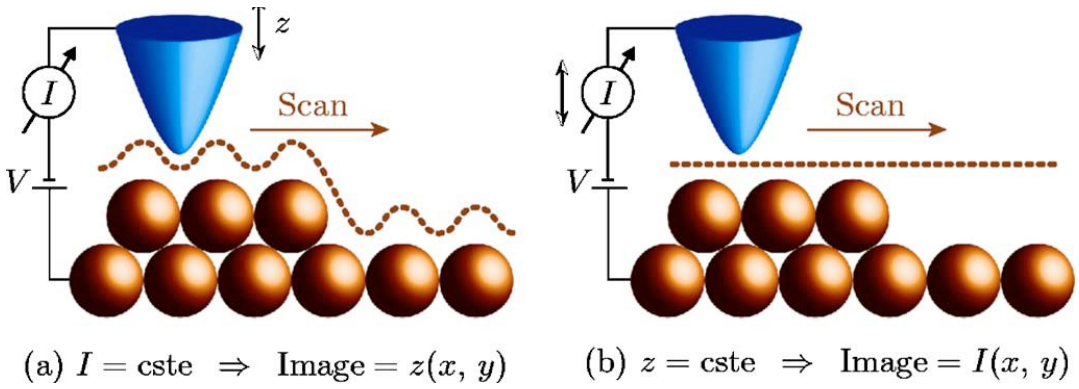

Figure 2.3: Two scanning configurations, (a) constant current and (b) constant STM tip height [29].

The usual expression of the tunneling current and tunneling conductance is via the Fermi golden rule.

$$\frac{dI}{dV} = 2\pi \frac{e^2}{\hbar} |t|^2 N_{STM} N_{sample} \ , \tag{2.1}$$

where t is the tunneling matrix element and $N_{STM/(sample)}$ are the local density of states (LDOS) in the STM (sample). Assuming that the LDOS of the STM apparatus does not vary significantly with the voltage, measurement of the tunneling conductance gives a direct information about the sample.

In our work we use a more involved formula for the tunneling conductance (see Equation 1.2) which will be developed and explained in the next section. In our results, we checked the validity of the assumption that the STM LDOS does not contribute significantly to the tunneling conductance. Moreover, we analyzed the contribution of this nontrivial conductance expression with respect to the Fermi golden rule tunneling conductance expression in order to determine whether the use of a more complicated formula is necessary.

2.2 Tunneling current and conductance

Our purpose is to evaluate the tunneling current (and the conductance) while taking into account the interaction due to tunneling between the STM tip and the sample. We will start with a general calculation done by [30]. The Hamiltonian can be written as:

$$\mathcal{H} = \mathcal{H}_R + \mathcal{H}_L + T \ , \tag{2.2}$$

where $\mathcal{H}_L$ ($\mathcal{H}_R$) represents the Hamiltonian of the STM (graphene with vacancy), and T represents the interaction between them via tunneling:

$$T = \sum_{l,r} T(r,l)\psi^{\dagger}(l)\psi(r) + H.c \ , \tag{2.3}$$

where l and r are locations in the left and the right regions respectively, $T(r,l)$ is the symmetric and real valued tunneling amplitude and $\psi^{\dagger}(l)$, $\psi(l)$ ($\psi^{\dagger}(r)$, $\psi(r)$) are creation and annihilation operators of the left (right) regions. When solving a tunneling problem, one can chose a configuration in a way that the many particle states are orthogonal but does not form a complete set [31]. In this case $[\mathcal{H}_R, \mathcal{H}_L] = 0$. Applying voltage at the left region creates a steady tunneling current:

$$I = e\left\langle \dot{N}_R \right\rangle \ . \tag{2.4}$$

After some involved algebra (see Appendix A.1.1) we get:

$$I = \frac{e}{h}\int d\omega \Re Tr G^K(\omega) \ , \tag{2.5}$$

where G^K is the Keldysh matrix Green's function whose definition in the time domain is:

$$G^K(r,l,t) = -i < [\psi(r,t), \psi^{\dagger}(l,0)] > \ . \tag{2.6}$$

The average $< ... >$ is thermodynamic with respect to $\mathcal{H}$ (original Hamiltonian), and the trace is done on all sites in the left and right regions (l, r). We would like to describe G^K as a function of the non interacting Green's functions of the left and right sides G_L, G_R. To this purpose [30] assumed that the potential behaves as depicted (see Figure 2.3), e.g that the voltage drop is only at the barrier so both sides are in thermal equilibrium.

The chemical potential is defined here by $\mu_R \equiv 0$, $\mu_L = eV$, therefore the Fermi distribution is $f_R(\omega) = f(\omega) = [1+\exp\beta\omega]^{-1}$, $f_L(\omega) = f(\omega - eV)$. Using this convention, the spectrum of the left side is shifted by eV, so that the left side Green's function $G_L^{\pm}(\omega) = G_{L,0}^{\pm}(\omega - eV)$, where $G_{L,0}^{\pm}(\omega)$ is the left side Green's function without bias.

In order to consider all possible interactions between the two regions in terms of propagators, we take all the paths between the two regions using the Dyson equation:

$$G = G_R T G_L + G_R T G_L T G_R T G_L + ... \tag{2.7}$$

Summing the geometric series and expressing the matrix elements of G using G^K, G^R, G^A of the isolated left and right regions (see Appendix A.1.2) we deduce:

$$\begin{aligned} TG^K = &\left(I - TG_R^+ TG_L^+\right)^{-1} \left[\left(1 - 2f_L(\omega)\right) TG_R^+ T\left(G_L^+ - G_L^-\right)\right. \\ &\left. + \left(1 - 2f_R(\omega)\right) T\left(G_R^+ - G_R^-\right) TG_L^-\right] \left(I - TG_R^- TG_L^-\right)^{-1} \end{aligned} \tag{2.8}$$

and the current:

$$\begin{aligned} I = \frac{e}{\hbar}\int \frac{d\omega}{2\pi} Tr\Re &\left(I - TG_R^+ TG_L^+\right)^{-1} \left[\left(1 - 2f_L(\omega)\right) TG_R^+ T\left(G_L^+ - G_L^-\right)\right. \\ &\left. + \left(1 - 2f_R(\omega)\right) T\left(G_R^+ - G_R^-\right) TG_L^-\right] \left(I - TG_R^- TG_L^-\right)^{-1} \quad . \end{aligned} \tag{2.9}$$

The conductance $\sigma = \frac{dI}{dV}$ has two contributions. One from the dependence of $f_L(\omega)$ on the voltage - $\tilde{\sigma}(V)$ - and the other from the voltage dependence of $G_L(\omega)$ - $\delta\sigma(V)$. Since the left side L represent the measurement apparatus, we assume that its dependence on the voltage is much smaller than the one of $f_L(\omega)$, so from the conductance expression:

$$\sigma(V) = \tilde{\sigma}(V) + \delta\sigma(V) \quad , \tag{2.10}$$

we can neglect $\delta\sigma(V)$ and obtain

$$\begin{aligned} \tilde{\sigma}(V) = \frac{e^2}{h}\int d\omega(-2f'(\omega - eV))\Re Tr[TG_R^+ T(G_L^+ - G_L^-)] \\ (I - TG_R^- TG_L^-)^{-1}(I - TG_R^+ TG_L^+)^{-1} \quad . \end{aligned} \tag{2.11}$$

At low temperature $-f(\omega - eV) \to \delta(\omega - eV)$, so the integral vanishes:

$$\tilde{\sigma}(V) = \frac{2e^2}{h}\Re Tr\left[TG_R^+(eV)\,T\left(G_{L,0}^+(0) - G_{L,0}^-(0)\right)\right] \left(I - TG_R^-(eV)\,TG_{L,0}^-(0)\right)^{-1}\left(I - TG_R^+(eV)\,TG_{L,0}^+(0)\right)^{-1} . \tag{2.12}$$

The setup we describe is constructed from STM as the measurement instrument (L) and graphene with vacancy (R) as the sample. We assume that electrons can tunnel only from the STM tip to the vacancy - a.k.a point contact:

$$T(\boldsymbol{l}, \boldsymbol{r}) = t\delta_{l,l_0}\delta_{r,r_0} , \tag{2.13}$$

where l_0 = STM tip, r_0 = graphene vacancy. Implementing this into (Equation 2.12) gives:

$$\tilde{\sigma}(V) = \frac{2e^2}{h}\Re Tr\left[t^2 G_R^+(r_0, r_0, eV)\left(G_{L,0}^+(l_0, l_0, 0) - G_{L,0}^-(l_0, l_0, 0)\right)\right] \left(1 - t^2 G_R^-(r_0, r_0, eV)\,G_{L,0}^-(l_0, l_0, 0)\right)^{-1}\left(1 - t^2 G_R^+(r_0, r_0, eV)\,G_{L,0}^+(l_0, l_0, 0)\right)^{-1} . \tag{2.14}$$

We use the relation between the local density of states and the Green's function (see Appendix A.3):

$$N_L(l_0, \omega) = \frac{1}{2\pi i}\left[G_L^-(l_0, l_0, \omega) - G_L^+(l_0, l_0, \omega)\right] \tag{2.15}$$

$$N_R(r_0, \omega) = -\frac{1}{\pi}\Im G_R^+(r_0, r_0, \omega) \tag{2.16}$$

to obtain:

$$\tilde{\sigma}(V) = -\frac{e^2}{h}\frac{(2\pi)^2 t^2 N_{L,0}(l_0, 0)\,N_R(r_0, eV)}{\left|\left(1 - t^2 G_R^+(r_0, r_0, eV)\,G_{L,0}^+(l_0, l_0, 0)\right)\right|^2} . \tag{2.17}$$

2.3 Modeling the system

To further use the tunneling conductance formula, we need create a simplified model of STM and graphene (+ vacancy) Green's functions. Below, each component will be estimated and calculated. Since the experimental data is $\sigma(E)$, we are interested in the energy dependence for a fixed voltage difference,

$$\tilde{\sigma}(E) = -\frac{e^2}{h}\frac{(2\pi)^2 t^2 N_{STM,0}(E, l_0, 0)\,N_G(E, r_0, eV)}{\left|\left(1 - t^2 G_G^+(E, r_0, r_0, eV)\,G_{STM,0}^+(E, l_0, l_0, 0)\right)\right|^2} . \tag{2.18}$$

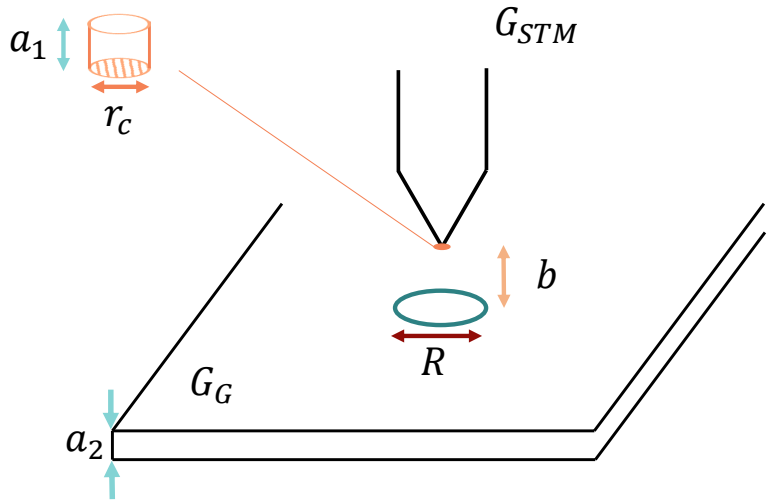

Figure 2.4: A schematic sketch of the setup. We approximate the STM tip to be a cylinder with radius r_c and width a_1. The distance between the tip and the vacancy is b, the radius of the vacancy is R. Finally, the width of the graphene sheet is a_2.

2.3.1 Evaluation of the tunneling matrix element

In order to calculate the tunneling matrix elements, we need to find the probability to overcome the potential barrier. To this purpose, the single particle wave function is approximated using the WKB method (a further explanation about this method can be found in [32]),

$$\begin{cases} \psi_1 = Ae^{i\kappa x} + Be^{-i\kappa x} & x < a_1 \\ \psi_2 = \frac{F}{\sqrt{|p(x)|}} e^{\frac{1}{\hbar}\int_{a_1}^{x}|p(x')|dx'} + \frac{G}{\sqrt{|p(x)|}} e^{-\frac{1}{\hbar}\int_{a_1}^{x}|p(x')|dx'} & a_1 < x < a_1 + b \\ \psi_3 = Ce^{ikx} & a_1 + b < x < a_1 + b + a_2 \end{cases} , \tag{2.19}$$

the momenta are defined by:

$$\begin{cases} p\left(a_1\right) = \sqrt{2m\left(E - V\left(a_1\right)\right)} \\ p\left(b + a_1\right) = \sqrt{2m\left(E - V\left(b + a_1\right)\right)} \\ \kappa = \frac{1}{\hbar}\sqrt{2m\left(E - V_0\right)} \\ k = \frac{1}{\hbar}\sqrt{2mE} \end{cases} . \tag{2.20}$$

In the matrix element along the z direction we assume free particles, and since we do not consider lateral confined motion within graphene, we assume a dispersion of free electrons. We demand continuity of the function and its derivative at points a_1 and

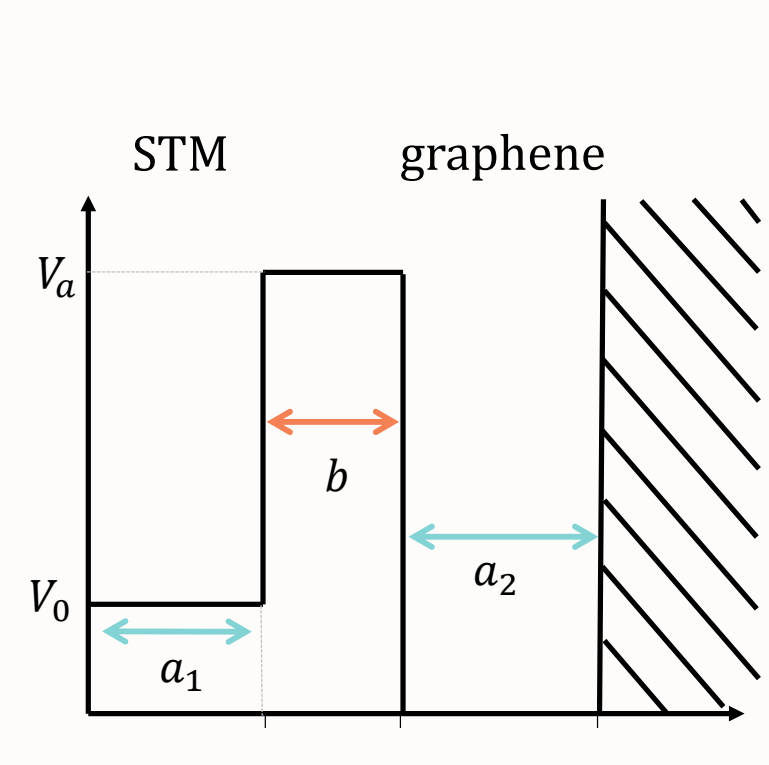

Figure 2.5: The potential as estimated in our model, on the left with width a_1 the STM measurement device. In the middle, the vacuum potential barrier with length b and on the right the sample with width a_2.

$a_1 + b$, with $e^{\tau} \equiv e^{\frac{1}{\hbar}\int_{a_1}^{b+a_1}|p(x')|dx'}$ and assume that $p'(x) \ll 1$, which means that the energy of the electron is much smaller than the potential barrier $V(b+a_1), V(a_1) \gg E$. We further assume $\tau \gg 1 \rightarrow \hbar \ll \int_{a_1}^{b+a_1} |p(x)|\, dx$. After some algebra (see Appendix A.2), we obtain the probability to overcome the potential barrier:

$$P_{pass} = \left|\frac{C}{A}\right|^2 = \frac{16\,(E-V_0)\sqrt{V(a_1)-E}}{(V(a_1)-V_0)\sqrt{V(b+a_1)-E}} e^{-2\tau} \quad . \tag{2.21}$$

Assuming further that $V(a_1) = V(b+a_1) = V_a$ gives:

$$P_{pass} = \frac{16\,(E-V_0)}{(V_a-V_0)} e^{-2\tau} \quad . \tag{2.22}$$

Our goal now is to relate the probability to overcome the potential barrier that we evaluated, to the tunneling matrix element. According to [33] the relation is:

$$\left|T_{k,k'}\right|^2 = P\frac{1}{LL'}\frac{\partial E}{\partial k}\frac{\partial E}{\partial k'} \quad , \tag{2.23}$$

where P is the tunneling probability, L and L' are the widths of the two metals (STM and graphene) and $(k,\, k')$ are the momenta of the two regions.

We assume free particles for both graphene and STM but shifted the energy of the STM, using the same notation as before (see Equation 2.20), for the STM:

$$\frac{\partial E}{\partial \kappa} = \frac{\hbar^2 \kappa}{m} = \frac{\hbar}{m}\sqrt{2m\left(E - V_0\right)} \ , \tag{2.24}$$

and for graphene:

$$\frac{\partial E}{\partial k} = \frac{\hbar^2 k}{m} = \frac{\hbar}{m}\sqrt{2mE} \ . \tag{2.25}$$

Plugging this into (Equation 2.23) gives:

$$\left|T_{\kappa,k}\right|^2 = P\frac{2}{a_1 a_2}\frac{\hbar^2}{m}\sqrt{E\left(E - V_0\right)} \ , \tag{2.26}$$

so that the tunneling probability is:

$$\left|T_{\kappa,k}\right|^2 = \frac{\hbar^2}{m a_1 a_2}\frac{32\left(E - V_0\right)}{\left(V_a - V_0\right)}\sqrt{E\left(E - V_0\right)}e^{-2\tau} \ . \tag{2.27}$$

For the final result, our definition of $\tau = \frac{1}{\hbar}\int_a^b \left|p\left(x'\right)\right| dx'$ can be expressed using the potential:

$$\tau = \frac{\sqrt{2m}}{\hbar}\sqrt{V_a - E}b \ , \tag{2.28}$$

so that:

$$\left|T_{\kappa,k}\right|^2 = \frac{\hbar^2}{m a_1 a_2}\frac{32\left(E - V_0\right)^{3/2}\sqrt{E}}{\left(V_a - V_0\right)}e^{-2\frac{\sqrt{2m}b}{\hbar}\sqrt{V_a - E}} \ . \tag{2.29}$$

2.3.2 Evaluation of the STM Green's function

In order to find the STM Green's function we used the spectral decomposition definition of Green's function:

$$G^{+}\left(r, r', E\right) = \sum_i \lim_{\epsilon \to 0}\frac{\psi_i^*\left(r'\right)\psi_i\left(r\right)}{E - E_i + i\epsilon} \ , \tag{2.30}$$

where ψ_i are the eigenfunctions of the STM isolated Hamiltonian and E_i are the corresponding energies. The original shape of the STM is a cone, but the interaction is only from the one-atom size tip edge. Therefore, we assume that the STM tip edge can be approximated by a circular well.

In order to find the eigenfunctions and the energy spectrum, we solve the problem of a particle in a two dimensions circular box (disregarding the z axis in this part). The single particle Schrödinger eq. is:

$$\left(-\partial_r^2 - \frac{1}{r}\partial_r + \frac{m^2}{r^2}\right)\phi\left(r\right) = \frac{2\mu E}{\hbar^2}\phi \ , \tag{2.31}$$

where the wavefunction is $\psi = \phi e^{im\theta}$. Changing the variables of the differential equation to $x = r\sqrt{\frac{2\mu E}{\hbar^2}}$ gives:

$$\left(x^2\partial_x^2 + x\partial_x - m^2 + x^2\right)\phi\left(x\right) = 0 \ , \tag{2.32}$$

a Bessel equation whose solutions are:

$$\phi_m\left(x\right) = A_m J_m\left(x\right) \ . \tag{2.33}$$

Since the wavefunction only exists inside the STM tip, we chose the boundary conditions:

$$\phi_m\left(r = r_c\right) = 0 = A_m J_m\left(r_c\sqrt{\frac{2\mu E}{\hbar^2}}\right) \ . \tag{2.34}$$

From the definition of Bessel function zeros we obtain the spectrum. If $J_m\left(u_{n,m}\right) = 0$, where $u_{m,n}$ is the n^{th} zero of the m^{th} Bessel function, then the energies are

$$E_{n,m} = \frac{\hbar^2}{2\mu}\left(\frac{u_{m,n}}{r_c}\right)^2 \ . \tag{2.35}$$

Normalizing states, $< n, m|n, m >= 1$, allows to obtain the coefficients A_m:

$$\left|A_{m,n}\right|^2 = \frac{1}{\pi r_c^2\left[J_{m+1}\left(u_{m,n}\right)\right]^2} \ . \tag{2.36}$$

According to the 'point contact' assumption, electrons can tunnel from a single point in the STM - the center of the tip. Therefore, the tunneling point is at $l_0 = 0$. The Green's function is evaluated at this point as well,

$$G^+_{STM}\left(0, 0, E\right) = \sum_{m,n}\frac{\left|\psi_{m,n}\left(0\right)\right|^2}{E - \frac{\hbar^2}{2\mu}\left(\frac{u_{m,n}}{r_c}\right)^2 + i\epsilon} \ . \tag{2.37}$$

However, since the Green's function is ill defined at $r = r'$, we take $r = 0$ and $r' = \epsilon_r \to 0$ and obtain:

$$G^+_{STM}\left(0, 0, E\right) = \sum_{m,n}\frac{\psi^*_{m,n}\left(\epsilon_r\right)\psi_{m,n}\left(0\right)}{E - \frac{\hbar^2}{2\mu}\left(\frac{u_{m,n}}{r_c}\right)^2 + i\epsilon} \ . \tag{2.38}$$

In addition, defining ($\vec{r} = re^{i\theta}$, $\vec{r}' = r'e^{i\theta'}$) and assuming that $\theta = \theta' = 0$ the angular contribution to the STM Green's function is vanishing:

$$G^+_{STM}\left(0, \epsilon_r, E\right) = \sum_{m,n}\frac{\phi^*_{m,n}\left(\epsilon_r\right)\phi_{m,n}\left(0\right)}{E - \frac{\hbar^2}{2\mu}\left(\frac{u_{m,n}}{r_c}\right)^2 + i\epsilon} \ . \tag{2.39}$$

Inserting Bessel function solutions gives:

$$G^{+}_{STM}\left(0,\epsilon_r,E\right)=\sum_{m,n}\frac{\left|A_{m,n}\right|^2 J_m\left(\epsilon_r\frac{u_{m,n}}{r_c}\right)J_m\left(0\right)}{E-\frac{\hbar^2}{2\mu}\left(\frac{u_{m,n}}{r_c}\right)^2+i\epsilon}\ , \tag{2.40}$$

the double sum can be reduced using:

$$J_m\left(0\right)=\begin{cases}1 & m=0\\ 0 & m\neq 0\end{cases}\ , \tag{2.41}$$

so that the Green's function of the STM at the contact point is:

$$G^{+}_{STM}\left(0,\epsilon_r,E\right)=\sum_{n}\frac{\left|A_{0,n}\right|^2 J_0\left(\epsilon_r\frac{u_{0,n}}{r_c}\right)J_0\left(0\right)}{E-\frac{\hbar^2}{2\mu}\left(\frac{u_{0,n}}{r_c}\right)^2+i\epsilon}\ . \tag{2.42}$$

2.3.3 Graphene with vacancy Green's function

A previous work in our group [16] solved the problem of graphene with one vacancy using the effective Dirac Hamiltonian description:

$$\mathcal{H}=-i\boldsymbol{\sigma}\cdot\boldsymbol{\nabla}=\begin{pmatrix}0 & D\\ D^{\dagger} & 0\end{pmatrix}\ , \tag{2.43}$$

where $D=-i\partial_x-\partial_y=e^{-i\theta}\left(-i\partial_r-\frac{1}{r}\partial_\theta\right)$ and $\boldsymbol{\sigma}$ are the Pauli matrices $\boldsymbol{\sigma}=(\sigma_x,\sigma_y)$. The states $\psi\left(r\right)$ of graphene are spinors,

$$\psi\left(\boldsymbol{r}\right)=\begin{pmatrix}\psi^A\\ \psi^B\end{pmatrix}\ , \tag{2.44}$$

with $\psi^{A/B}$ being amplitudes on sublattice A or B respectively. The spatial Green's function obeys the equation:

$$\int d\boldsymbol{r}''\left\langle\boldsymbol{r}\left|H^{A/B}+z\right|\boldsymbol{r}''\right\rangle\left\langle\boldsymbol{r}''\left|G^{A/B}\right|\boldsymbol{r}'\right\rangle=\frac{1}{r}\delta\left(r-r'\right)\delta\left(\theta-\theta'\right)\ , \tag{2.45}$$

where $\sqrt{z}=\frac{E}{\hbar v_f}$ and $H^A=DD^{\dagger}$, $H^B=D^{\dagger}D$. Separating the radial and spherical coordinates leads to boundary conditions on the radial part of the Green's function,

$$G^{A/B}\left(\boldsymbol{r},\boldsymbol{r}'\right)=\frac{1}{2\pi}\sum_{m=-\infty}^{\infty}G^{A/B}_m\left(r,r'\right)e^{im(\theta-\theta')}\ . \tag{2.46}$$

Boundary conditions were chosen such that the vacancy behaves like a perfect scatterer [16]. Therefore, demanding the vanishing of the wave function probability density at the vacancy radius. Moreover, since a vacancy breaks the sublattice symmetry, the boundary

conditions differ between the two sublattices and thus break this symmetry. For a single A vacancy the boundary conditions of the Green's function are

$$\left(-\partial_r^2-\frac{1}{r}\partial_r+\frac{m^2}{r^2}+z\right)G_m^A\left(r,r'\right)=\frac{1}{r}\delta\left(r-r'\right),\quad\begin{cases}G_m^A\left(R,r'\right)=0 & \boldsymbol{m\leq 0}\\ \partial_r G_m^A\left(R,r'\right)/G_m^A\left(R,r'\right)=\frac{m}{R} & m>0\end{cases} \tag{2.47}$$

$$\left(-\partial_r^2-\frac{1}{r}\partial_r+\frac{m^2}{r^2}+z\right)G_m^B\left(r,r'\right)=\frac{1}{r}\delta\left(r-r'\right),\quad\begin{cases}G_m^B\left(R,r'\right)=0 & \boldsymbol{m<-1}\\ \partial_r G_m^B\left(R,r'\right)/G_m^B\left(R,r'\right)=\frac{m}{R} & m\geq -1\end{cases} \tag{2.48}$$

and the solutions are the first and second kind modified Bessel functions:

$$G_{m,\,\text{graphene}}^{A/B}=I_m\left(\sqrt{z}r_<\right)K_m\left(\sqrt{z}r_>\right)+\Gamma_m^{A/B}K_m\left(\sqrt{z}r\right)K_m\left(\sqrt{z}r'\right)\ , \tag{2.49}$$

where $r_<\equiv\min(r,r')$, $r_>\equiv\max(r,r')$ and with the nontrivial coefficients (the only modes where $G_m^A\neq G_m^B$):

$$\begin{cases}\Gamma_0^A=-\Gamma_{-1}^B=-\frac{I_0\left(\sqrt{z}R\right)}{K_0\left(\sqrt{z}R\right)}\\ \Gamma_0^B=-\Gamma_{-1}^A=\frac{I_1\left(\sqrt{z}R\right)}{K_1\left(\sqrt{z}R\right)}\\ \Gamma_m^A=\Gamma_m^B\ \text{for}\ m>0\end{cases}. \tag{2.50}$$

Breaking of parity symmetry between the two sublattices, leads to a charge accumulation around the vacancy. Using the spectral decomposition, the boundary conditions determine the behavior of each mode. In some modes the boundary condition discriminates between A and B sublattices. The accumulated charge is caused by the differences in the sublattices, therefore the modes relevant to us are those such that $G_m^A\neq G_m^B$, namely $m=0,-1$.

$$G_0^B\left(R,R\right)=\frac{K_0\left(\sqrt{z}R\right)}{\sqrt{z}RK_1\left(\sqrt{z}R\right)} \tag{2.51}$$

$$G_{-1}^B\left(R,R\right)=\frac{K_1\left(\sqrt{z}R\right)}{\sqrt{z}RK_0\left(\sqrt{z}R\right)} \tag{2.52}$$

Furthermore, in these modes ($m=0,\ -1$) the Green's function of sublattice A vanishes. This result is very reassuring, since the point contact approximation prevents most of the tunneling paths, allowing tunneling to a single point on graphene lattice - at the vacancy radius. In the case of a A sublattice vacancy (our case) the vacancy radius contains only B sites (see Figure 2.6). Hence, in our calculations we take $G_{0,\,-1}^B$ to represent the Green's function of graphene with a vacancy.

2.4 Numerical calculations and results

So far have derived an analytic expression of all the different terms in the conductance formula. The next step is to perform a numerical evaluation of each term separately. Though, for now we show the relation between the imaginary part of the Green's function to the local density of states (see proof in Appendix A.4) :

$$N\left(r_0,\omega\right)=-\frac{1}{\pi}\Im G^{+}\left(r_0,r_0,\omega\right)\quad . \tag{2.53}$$

Next we consider all the parameters, both estimated and determined from the experiment. For convenience, we divide them into subgroups, first are the parameters obtained from the measurement setup:

- $V_0 = 2\text{meV}$ the voltage difference amplitude applied in the experiment (see supplementary material in [15]).
- $b = 0.1\text{nm}$ the distance between the STM tip edge and graphene vacancy. [14] analysed the measured signal with respect to the distance, therefore the value of b is in agreement with this experiment.

Next, there are parameters we had to estimate:

- l_0 is the site on the STM electrons can hop to (or from). Since the STM tip contains one atom, this site is taken to be $l_0 = 0$ - exactly at the center of the tip.
- r_0 is the site on graphene lattice electrons can hop to, which is the vacancy radius, therefore $r_0 = R$ where R is the vacancy radius.
- $R = 142\text{pm}$ the vacancy radius is taken to be the graphene lattice constant (see Figure 2.6).
- $a_1 = a_2 = 140\text{pm}$ are the widths of the graphene layer and of the STM tip. The STM tip is of the order of a single atom and since graphene is a two dimensional lattice, its width is on the scale of a single atom.
- $r_c = 139\text{pm}$ is the radius of the STM tip, and it is also on the scale of a single atom.
- $V_a = 7.64\text{eV}$ the height of the potential well barrier (see Figure 2.5). Its value is taken to be the ionization energy of graphene.

The two last parameters were inserted from numerical reasons:

- $\epsilon_E = 0.01\text{meV}$ the δE steps of the energy values in our plots.

- $\epsilon_r = 210^{-3} r_c$ the distance between r and r'. Inserting this parameter helps the STM Green's function to numerically converge. The effect of this parameter is irrelevant, and in order to show this we have taken different values of ϵ_r and show that the corresponding data remain unchanged.

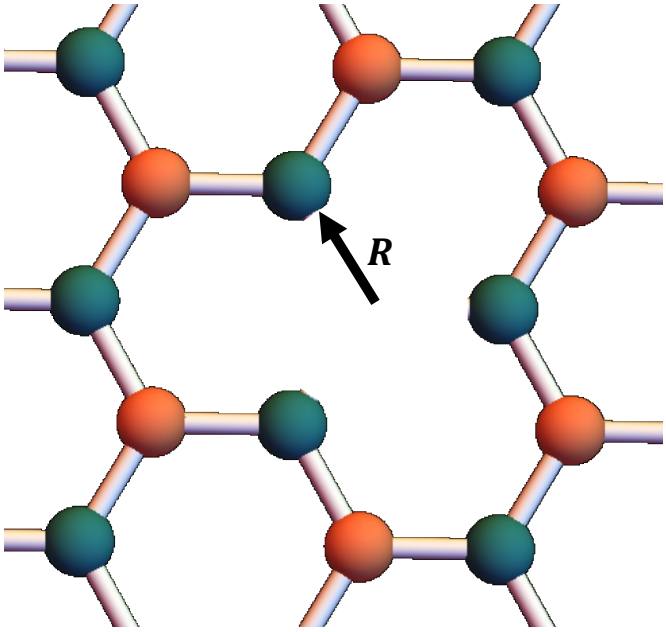

Figure 2.6: In the case of A vacancy, the vacancy radius only has B sites. In addition, the vacancy radius R is precisely the lattice constant of graphene.

The dependence of each term upon the different variables is mentioned,

$$\sigma(E) = \frac{e^2}{h} \frac{(2\pi t(E, V_a, V_0, b))^2 N_G(R, E) N_{STM}(0, r_\epsilon, r_c, E)}{\left|1 - t^2(E) G^+_{STM}(0, r_\epsilon, r_c, E) G^+_G(R, E)\right|^2} . \tag{2.54}$$

Our results (see Figure 2.7) are obtained using Matlab for a numerical evaluation of this expression. As expected, we observed a sizeable shift from zero, that is obtained by inserting in our model the interaction of graphene with the measurement instrument. STM is a measurement device based on tunneling electrons, so that to obtain measurable data the tunneling current must be large enough. Therefore, the tunneling interaction term, which enables the tunneling current, can not be neglected. This term has an energy scale which can explain the shifted zero mode peak and the σ_3 symmetry breaking. The numerical value of the shifted peak is $\simeq 2.3$meV and the experimentally measured value is 8.3meV (see Figure 2.8). These two values are of the same order of magnitude, which is surprising considering the variety of parameters we had to estimate.

Separating the tunneling conductance term into a numerator and a denominator (see Figure 2.9) and analyzing the behavior of each part, we can notice that the shifted

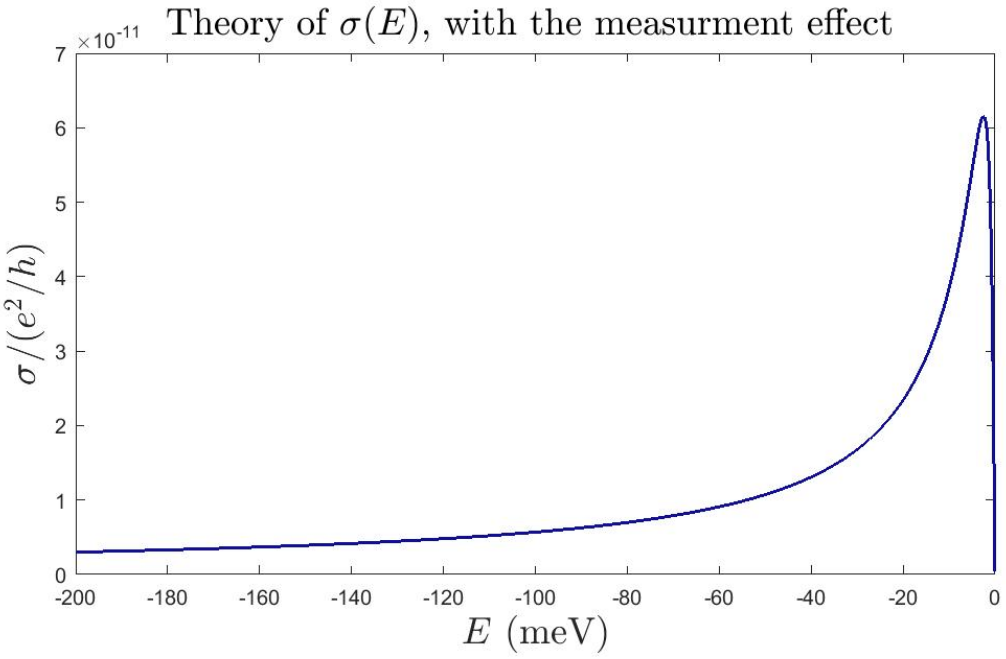

Figure 2.7: Numeric results of the conductance due to tunneling current. We can see that as expected, that the peak is not exactly at zero but shifted a bit. $V_0 = 2$meV, $\epsilon_E = 0.01$meV, $R = 142$pm, $V_a = 7.64$eV, $b = 0.1$nm, $a_1 = a_2 = 140$pm, $r_c = 139$pm, $\epsilon_r = 2r_c 10^{-3}$

peak is due to the denominator. Whose origin is the sum (a geometric series) over all the possible tunneling paths (2.7), instead of taking just the first term that yields the numerator. Remember that the numerator is simply the Fermi golden rule based tunneling conductance expression, which can not explain the shifted peak. However, the shifted zero mode can be explained by the more involved expression we used. In order to better understand the formation of the denominator peak, we further examine it behavior using the function $f(E)$ (the denominator)

$$f(E) = |1 - |t|^2 G^+_{STM} G^+_G|^2 \tag{2.55}$$

such that it should have a minima when $1/|1 - |t|^2 G^+_{STM} G^+_G|^2$ obtains it maximum value. When writing $f(E)$ as:

$$f(E) = 1 - 2|t|^2 Re(G^+_{STM} G^+_G) + |t|^4 |G^+_{STM}|^2 |G^+_G|^2 \ , \tag{2.56}$$

numerically the second term $-2t^2 Re(G^+_{STM} G^+_G)$ does not contribute to the peak location. This somewhat surprising result origins in the large value of G_{STM} compered with $|t|^2$. Therefore, for analytic convenience we neglect this term and left with

$$f(E) = 1 + |t|^4 |G^+_{STM}|^2 |G^+_G|^2 \ . \tag{2.57}$$

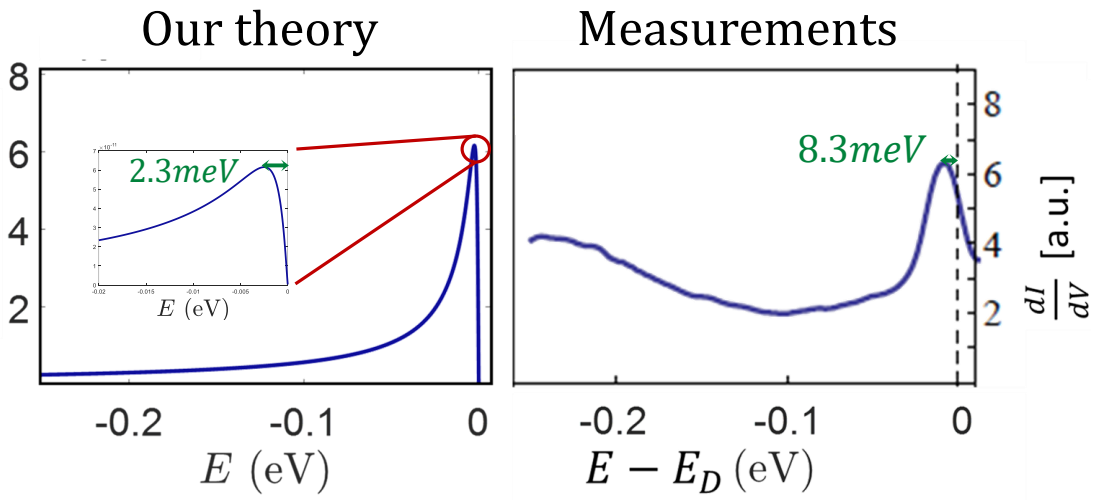

Figure 2.8: Numerical results of (left) our energy value of the shifted peak $\simeq$ 2.3meV and (right) the measured value $\simeq$ 8.3meV. Both are of the same order of magnitude.

Next, the location of the extremum is determined by the derivative of $f(E)$ with respect to the energy, which can be written as

$$\frac{df(E)}{dE} = 2|t|^4 |G^+_{STM}|^2 |G^+_G|^2 \, (2\frac{t'}{t} + Re\frac{G^{+\prime}_G}{G^+_G}) \ . \tag{2.58}$$

The energy scale E_0 for which $\frac{df}{dE}$ vanishes is provided by the equation

$$2\frac{t'}{t} + Re\frac{G^{+\prime}_G}{G^+_G} = 0 \tag{2.59}$$

which can be written as

$$\frac{d}{dE} \ \ln\left(t^2\sqrt{(\Im G^+_G)^2 + (\Re G^+_G)^2}\right) \ = 0 \tag{2.60}$$

suggesting that the energy scale from the denominator is determined by both the imaginary and real part of graphene Green's function. Numerically neglecting one of them changes the peak location of the denominator. Considering our results there are several observations that can be made:

1. $|t|^2 \neq 0$ is a necessary condition to have $\sigma \neq 0$.

2. Characteristic energy shift $\propto |t|^2$ but more precisely to $|t|^2 G^+_{graphene} G^+_{STM}$.

3. $G^+_{graphene}$ involves the specific features of the chiral boundary conditions due to vacancies.

4. Truncation of the Dyson equation prevents inserting full information about

$G^{+}_{graphene}$. For example, truncating the series after the first term (direct tunneling) leads to the "text book" expression which contains only the Green's function imaginary part, such that the information regarding the real part was lost.

5. If G_{sample} does not describe some exotic behavior such as graphene with vacancies this additional information might be unnecessary.

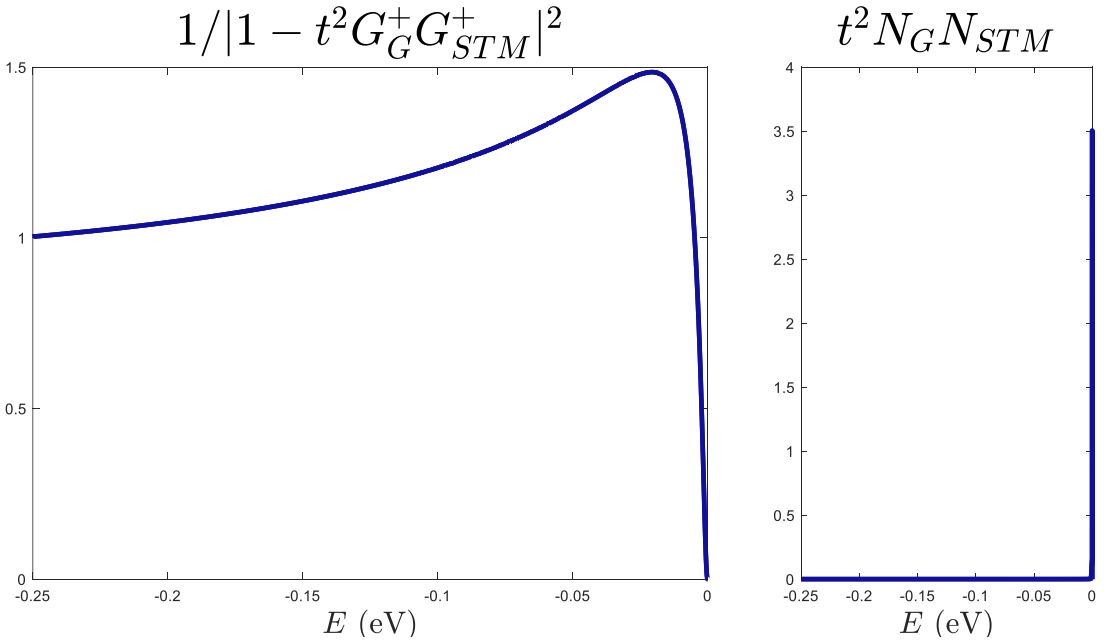

Figure 2.9: Comparison between the contribution of the (left) denominator and the (right) numerator in the conductance expression, in arbitrary units (a.u). The shifted peak results from the denominator.

Next, we examine the assumption that the tunneling conductance gives a direct information about the local density of states in the measured sample. Therefore assuming that the energy dependence of the STM itself is insignificant in comparison to the sample dependence. We checked the validity of this assumption by removing entirely the STM Green's function dependence in the energy (see Figure 2.10) and observed that indeed, the energy dependence of the STM Green's function negligible. Therefore, in our case this assumption is valid.

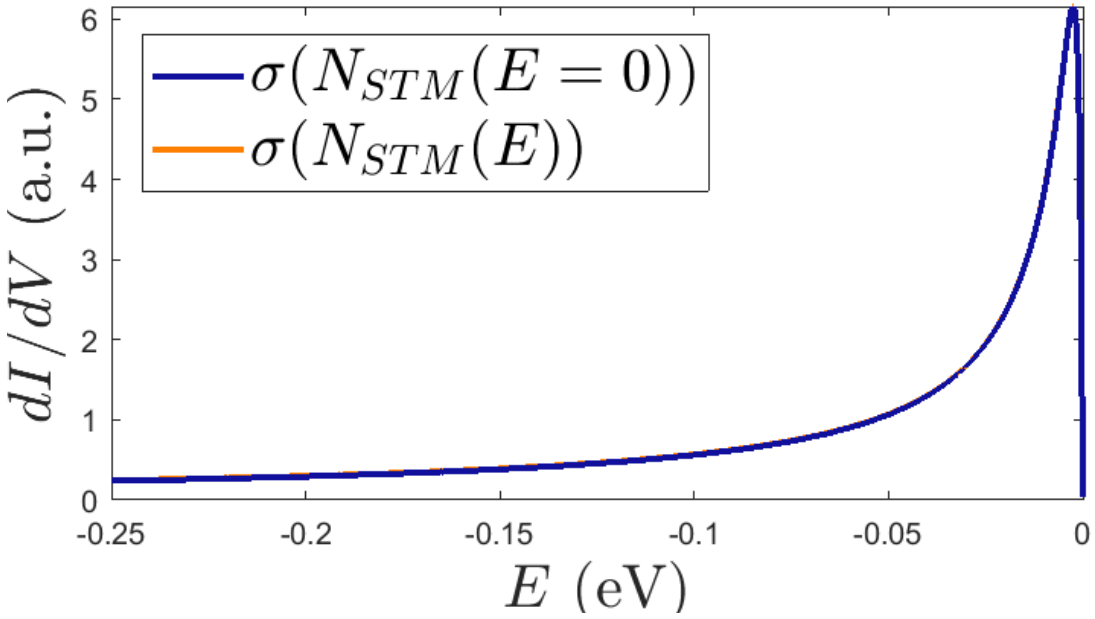

Figure 2.10: Dependence of the change in the tunneling conductance by removing the energy dependence of the STM Green's function. It is clear that assuming $N_{STM}(E=0)$ does not change the tunneling conductance results.

Chapter 3

Mapping to a Simplified problem

We would like to further investigate graphene with vacancies. Mostly, its peculiar but highly interesting behavior under high voltage pulses. Graphene with one vacancy, in our current knowledge, is represented by Dirac equation with chiral boundary conditions on the edge of the vacancy. This description is ratter limiting, generalization to many vacancies is not easy and its behavior under time dependent potential (high voltage pulses) is difficult to analyze. Our main goal here is to predict the charge accumulation around the vacancy in the presence of high voltage pulses. Therefore, we propose a mapping to a simplified system without a vacancy.

3.1 Analogy between two systems

Let us stress again the physical features of graphene with vacancies [16]:

1. The number of additional zero energy modes is $\# = |N_A - N_B|$.
2. The total charge in the lattice can be fractional $Q = -\frac{e}{2}(N_A - N_B)$.
3. Parity symmetry breaking (under parity transformation $Q \to -Q$).

These physical features also appear in a different formal problem. Hence, this system may be related to graphene with vacancies. Our goal here is to present our current and future work regarding this connection between the two systems. The second problem, one with Dirac field interacting with complex scalar field and axial gauge field, exhibits the following features [34]:

1. There are $|n|$ zero energy solutions.
2. The total charge is $Q = -\frac{e}{2}\, n\, sign(\mu)$.
3. Under parity transformation $Q \to -Q$,

where n the integer is related to the static background scalar and gauge fields:

$$\varphi(\boldsymbol{r}) = \phi(r)e^{in\theta} \ , \tag{3.1}$$

$$A_5^i = -n\epsilon^{ij}\frac{r^j}{r^2}a(r) \ , \tag{3.2}$$

and $a(r)$ goes to $\frac{1}{2}$ for large r and $\phi(r)$ vanishes as $r^{|n|}$ and goes to a constant ϕ_0 at infinity [35]. The Hamiltonian density that exhibits these three physical features is:

$$\mathcal{H} = \psi^\dagger[\boldsymbol{\alpha}\cdot(\boldsymbol{p} - \gamma_5\boldsymbol{A}_5) + \beta(\varphi_1 - i\gamma_5\varphi_2) + R\mu]\psi \ , \tag{3.3}$$

where $\varphi = \varphi_1 + i\varphi_2$ is a complex scalar field, ($\psi^\dagger$, ψ) are creation and annihilation operators for fermion Dirac field (four component), $\boldsymbol{A}_5$ is the axial gauge field and the matrix:

$$\boldsymbol{\alpha} = (\alpha^x, \alpha^y) \equiv \begin{pmatrix} \boldsymbol{\sigma} & 0 \\ 0 & -\boldsymbol{\sigma} \end{pmatrix}, \beta = \begin{pmatrix} 0 & 1 \\ 1 & 0 \end{pmatrix}, \gamma_5 = -i\alpha^x\alpha^y\alpha^z = \begin{pmatrix} 1 & 0 \\ 0 & -1 \end{pmatrix} \ , \tag{3.4}$$

$$\alpha^z = \begin{pmatrix} \sigma_3 & 0 \\ 0 & -\sigma_3 \end{pmatrix} \ . \tag{3.5}$$

Although these two systems have common physical features, the Hamiltonian density (3.3) has an axial symmetry that graphene with vacancies does not have. Moreover, the origin of this Hamiltonian (3.3) (presented in the coming subsections) is from graphene with a Kekulé distortion. Scattering calculations of graphene with a Kekulé distortion, compared with vacancies give a different result [36]. Thus, our goal is to locate the origin of the axial symmetry, remove it and recalculate all the relevant properties (total charge, charge density, number of zero modes, etc.). Assuming that when the symmetries describing both system are the same, we could create a mapping between them.

3.2 Spinor and scalar fields interactions

Looking for the axial symmetry, we found its origin in the Hamiltonian of graphene with the tight binding approximation. However, instead of a constant hopping coefficient, small fluctuations are now allowed [37]. These fluctuations are directly related to the complex scalar field (3.1) and the fermion field originate from the description of graphene using an effective non-interacting Dirac field.

The addition of interactions with scalar field that contains topological background, leads to the appearance of interesting features. First, we address the case of interactions between spinor and scalar fields without vector field as done in [37], and relate the complex scalar field to the hopping amplitude fluctuations at the tight biding model.

The Hamiltonian of graphene with a hopping term that contains small fluctuations in [37]:

$$H = -\sum_{\boldsymbol{r}\in\Lambda_A}\sum_{i=1}^{3}\left(t+\delta t_{\boldsymbol{r},i}\right)a_{\boldsymbol{r}}^{\dagger}b_{\boldsymbol{r}+\boldsymbol{s}_i}+h.c.\ , \tag{3.6}$$

where $a_{\boldsymbol{r}}$ and $a_{\boldsymbol{r}}^{\dagger}$ ($b_{\boldsymbol{r}}$ and $b_{\boldsymbol{r}}^{\dagger}$) are annihilation and creation operators of sublattices A (B). $\boldsymbol{s}_i$ $(i=1,2,3)$ is a vector that connects a site on sublattice A to its nearest neighbors and $t((r)=t+\delta t_{\boldsymbol{r},i}$ is the hopping amplitude. The insertion of a Kekulé texture in [37] couples the two Dirac points $K_{\pm}=\pm\left(\frac{4\pi}{3\sqrt{3}a},0\right)$ such that the hopping term specific spatial dependence is:

$$\delta t_{\boldsymbol{r},i}=\Delta\left(\boldsymbol{r}\right)e^{i\boldsymbol{K}_{+}\cdot\boldsymbol{s}_i}e^{i\boldsymbol{G}\cdot\boldsymbol{r}}+c.c\ , \tag{3.7}$$

with $\boldsymbol{G}=\boldsymbol{K}_{+}-\boldsymbol{K}_{-}$. In the case $\Delta(\boldsymbol{r})$ is constant (or has an expectation value), a gap is created in the spectrum and effective mass is induced. Furthermore, in order for charge fractionalization to emerge, $\Delta(\boldsymbol{r})$ must contain vortices:

$$\Delta\left(\boldsymbol{r}\right)=\Delta_0\left(r\right)e^{i(\alpha+n\theta)}\ . \tag{3.8}$$

The Kekulé distortion term $e^{i\boldsymbol{K}_{+}\cdot\boldsymbol{s}_i}e^{i\boldsymbol{G}\cdot\boldsymbol{r}}$ connects between the two Dirac points (see

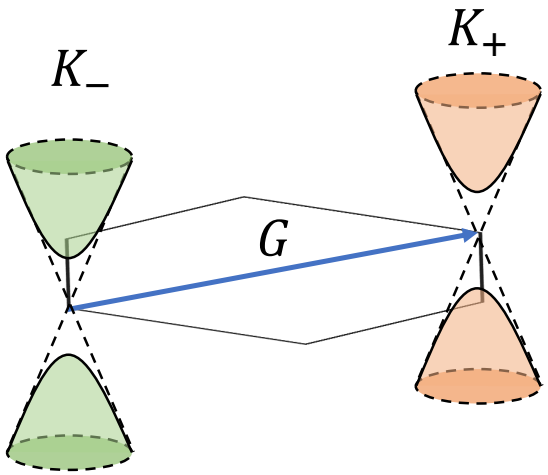

Figure 3.1: In [37] graphene Brillouin zone with two Dirac points K_+ and K_- coupled by G. The Dirac cone (dashed line) is changed and a gap is added by the Kekulé texture that mixes the $+-$ points and induce a mass term.

Figure 3.1), which is the origin of the axial symmetry we would like to remove. Therefore, for now we present the derivation of the axial symmetry from the Kekulé distortion term.

Expanding the Hamiltonian around the points K_+ and K_-, such that the creation and annihilation operators around these point are $a_\pm(\boldsymbol{p}) = a(\boldsymbol{K}_\pm + \boldsymbol{p})$, $b_\pm(\boldsymbol{p}) = b(\boldsymbol{K}_\pm + \boldsymbol{p})$ and the Hamiltonian is [35]:

$$H = \int d^2 r \Psi^*(r) K \Psi(r) \quad , \tag{3.9}$$

with

$$K = \begin{pmatrix} 0 & p_x - ip_y & \Delta(\boldsymbol{r}) & 0 \\ p_x + ip_y & 0 & 0 & \Delta(\boldsymbol{r}) \\ \Delta^*(\boldsymbol{r}) & 0 & 0 & -(p_x - ip_y) \\ 0 & \Delta^*(\boldsymbol{r}) & -(p_x + ip_y) & 0 \end{pmatrix} \quad , \tag{3.10}$$

$$\Psi = \begin{pmatrix} \psi_+^b \\ \psi_+^a \\ \psi_-^a \\ \psi_-^b \end{pmatrix} \quad , \tag{3.11}$$

with the definition of $\psi_\pm^a = \int d^2 p e^{-i\boldsymbol{p}\cdot\boldsymbol{r}} a_\pm(p)$, $\psi_\pm^b = \int d^2 p e^{-i\boldsymbol{p}\cdot\boldsymbol{r}} b_\pm(p)$.

It was shown in [37] that when the vortices are far apart, each vortex carries an energy zero mode, such that there are n zero modes in total. This is the first physical feature in common with vacancies in graphene.

3.3 Spinor scalar and vector fields

A suggestion made in [35] notes that this vortex is a Landau, Ginsburg, Abrikosov vortex which is also described by complex scalar field. However, when a U(1) gauge field is involved the creation energy of the vortex is finite. Thus, a chiral coupling of the gauge and spinor fields was suggested.

We notice that the Hamiltonian equation (3.9) can be written as:

$$\Psi^*(r) K \Psi(r) = \Psi^*(r) \begin{pmatrix} \boldsymbol{\sigma}\cdot\boldsymbol{p} & \Delta(\boldsymbol{r}) \\ \Delta^*(\boldsymbol{r}) & -\boldsymbol{\sigma}\cdot\boldsymbol{p} \end{pmatrix} \Psi(r) \quad . \tag{3.12}$$

We denote $\Delta(\boldsymbol{r}) = g\varphi(\boldsymbol{r}) = g(\varphi_1 + i\varphi_2)$ as the scalar field φ and its coupling strength g. After some algebra (see Appendix A.4) we get:

$$\Psi^*(r) K \Psi(r) = \Psi^*(r) (\boldsymbol{\alpha}\cdot\boldsymbol{p} + g\beta(\varphi_1 - i\varphi_2\gamma_5)) \Psi(r) \quad , \tag{3.13}$$

where $\boldsymbol{\alpha} = \begin{pmatrix} \boldsymbol{\sigma} & 0 \\ 0 & -\boldsymbol{\sigma} \end{pmatrix}$, $\beta = \begin{pmatrix} 0 & I \\ I & 0 \end{pmatrix}$, $\gamma_5 = -i\alpha^1\alpha^2\alpha^3 = \begin{pmatrix} I & 0 \\ 0 & -I \end{pmatrix}$.

The interaction term can be written as (see Appendix A.4):

$$\Psi^{*}\beta\left(\varphi_{1}-i\gamma_{5}\varphi_{2}\right)\Psi=\left|\varphi\right|\Psi^{*}\beta e^{-i\gamma_{5}\chi}\Psi\ \ , \tag{3.14}$$

where the complex scalar field is $\left|\varphi\right|e^{i\chi}=\varphi=\varphi_{1}+i\varphi_{2}$. Therefore, under the local chiral gauge transformation:

$$\begin{gathered}\varphi\rightarrow e^{2i\omega}\varphi\Rightarrow\chi\rightarrow\chi+2\omega,\\ \Psi\rightarrow e^{i\omega\gamma_{5}}\Psi,\end{gathered}$$

the interaction term is invariant (see Appendix A.4). Thus, the Kekulé distortion keeps the axial symmetry. Furthermore, the coupling of Dirac fermions to a gauge field in the case of axial symmetry, is done using an axial gauge field, such that the entire Hamiltonian is invariant under this transformation,

$$A_{i}\rightarrow\left(A_{i}+\partial_{i}\omega\right)\ \ ,$$

$$\Psi^{*}\left(r\right)K\Psi\left(r\right)=\Psi^{*}\left(r\right)\left(\alpha^{i}\left(p_{i}-\gamma_{5}A_{i}\right)+g\left|\varphi\right|\beta e^{-i\gamma_{5}\chi}\right)\Psi\left(r\right)\ \ . \tag{3.15}$$

Up to now, we presented the derivation of the Hamiltonian and found the origin of the axial symmetry. In future calculations, our definition of the hopping term fluctuations will neglect the Kekulé distortion from $\delta t(r)$ such that equation (3.7) becomes:

$$\delta t_{\boldsymbol{r},i}=\Delta\left(\boldsymbol{r}\right)+c.c \tag{3.16}$$

while keeping the topological behavior of $\Delta\left(\boldsymbol{r}\right)$:

$$\Delta\left(\boldsymbol{r}\right)=\Delta_{0}\left(r\right)e^{i(\alpha+n\theta)}\ \ . \tag{3.17}$$

Therefore, preserving the topological solution of the scalar field $\Delta\left(\boldsymbol{r}\right)=g\varphi\left(\boldsymbol{r}\right)=g\left(\varphi_{1}+i\varphi_{2}\right)$

$$\varphi(\boldsymbol{r})=\phi(r)e^{in\theta}\ \ , \tag{3.18}$$

the gauge field must remain unchanged,

$$A^{i}=-n\epsilon^{ij}\frac{r^{j}}{r^{2}}a(r)\ \ , \tag{3.19}$$

since in this form the energy cost to form a vortex is finite according to Landau, Ginsburg, Abrikosov equations.

We plan to redefine the Hamiltonian using the new definition of δt (without the axial symmetry) and recalculate all three features we previously discussed. Based on our suggested mapping, we might be able to solve the problem of vacancies in graphene

with a time dependent potential (i.e. with a high voltage pulses). Furthermore, this mapping might help to understand the reason why electrons rearrange themselves into new stable states after a high voltage pulses is applied.

Chapter 4

Conclusion and open questions

In our work we studied the behavior of graphene with vacancies under the influence of a measurement apparatus. Our main goal was to explain the source of the additional energy scale, that broke the symmetric spectrum by shifting the zero mode away from the Fermi energy. To that purpose, we proposed that the added energy scale is related to the tunneling interaction term between the STM and graphene lattice. We estimated the tunneling conductance behavior, while taking into account the Hamiltonian of the full system (graphene with vacancy, STM and the interaction between them). A numerical value for the energy shift from the Fermi energy has been obtained and compared with the measured data, and a good agreement is obtained.

We also highlighted the differences between two tunneling conductance expressions. One, is the 'text book' expression based on the Fermi golden role. Another, more involved expression we used, takes into consideration all tunneling paths through the potential barrier. In our results, it is clear that only the second expression can explain the shifted zero mode peak. Next, we examine the validity of an assumption that neglects the energy dependence of the measurement apparatus. According to our numerical calculation, this assumption is very good.

Finally, we suggested an approach for modeling graphene with vacancy using a mapping onto a fermion field interacting with gauge and scalar fields. This mapping was suggested as the first step to the solution of a complicated and yet fascinating problem, of a changing charged states due to high voltage pulses applied from the STM. This approach is not finished and will be part of future work.

However, we still wish to propose subjects to follow in future research. The first one is regarding a question about the bipartite nature of graphene. In our calculations we obtained $\simeq 2.3$meV as the shifted energy value. Since the next nearest neighbor hopping term is $\simeq 73$meV, a further analysis regarding the contribution of this term to the zero mode location is suggested. Moreover, another remaining question is related to lattice

deformation around the location of a vacancy. Vacancies in our model simply cause the removal of bonds in the Hamiltonian. Yet, some distortion of the atoms location around the vacancies may occur, which can change the local hopping coefficient of the next nearest neighbors.

Appendix A

Appendix

A.1 Tunneling conductance formula

A.1.1 Tunneling current

We wish to obtain the formula:

$$I = \frac{e}{h} \int d\omega \Re Tr G^k(\omega) \quad , \tag{A.1}$$

where the definition of the tunneling current is:

$$I = e \left\langle \dot{N}_R \right\rangle \tag{A.2}$$

and the number of particles in the right side is defined by $N_R = \sum_r \psi^\dagger(\boldsymbol{r})\psi(\boldsymbol{r})$. According to Ehrenfest theorem the time dependence of N_R is:

$$i\hbar \dot{N}_R = [N_R, \mathcal{H}] = [N_R, \mathcal{H}_R + \mathcal{H}_L + T] \quad , \tag{A.3}$$

remembering that $[H_L, H_R] = 0$ [31] the remaining part can be calculated:

$$\begin{aligned}
i\hbar\dot{N}_R &= \sum_{l,r} T(l,r)\left[N_R, \psi^\dagger(l)\psi(r) + \psi^\dagger(r)\psi(l)\right] \\
&= \sum_{l,r} T(l,r)\left[\sum_{r'} \psi^\dagger(r')\psi(r'), \psi^\dagger(l)\psi(r) + \psi^\dagger(r)\psi(l)\right] \\
&= \sum_{l,r,r'} T(l,r)\Big(\psi^\dagger(r')\psi(r')\psi^\dagger(l)\psi(r) - \psi^\dagger(l)\psi(r)\psi^\dagger(r')\psi(r') \\
&+ \psi^\dagger(r')\psi(r')\psi^\dagger(r)\psi(l) - \psi^\dagger(r)\psi(l)\psi^\dagger(r')\psi(r')\Big) \\
&= \sum_{l,r,r'} T(l,r)\Big(\psi^\dagger(l)\psi^\dagger(r')\psi(r')\psi(r) - \psi^\dagger(l)\Big(\delta_{r,r'} - \psi^\dagger(r')\psi(r)\Big)\psi(r') \\
&+ \psi^\dagger(r')\Big(\delta_{r,r'} - \psi^\dagger(r)\psi(r')\Big)\psi(l) - \psi^\dagger(r')\psi^\dagger(r)\psi(l)\psi(r')\Big) \\
&= \sum_{l,r,r'} T(l,r)\Big(-\psi^\dagger(l)\psi(r')\delta_{r,r'} + \psi^\dagger(r')\delta_{r,r'}\psi(l)\Big) \\
&= -\sum_{l,r'} T(l,r)\Big(\psi^\dagger(l)\psi(r) - \psi^\dagger(r)\psi(l)\Big) \quad . \qquad \text{(A.4)}
\end{aligned}$$

Simply, the extraction of $\dot{N}_R$ gives:

$$\dot{N}_R = \frac{i}{\hbar}\sum_{l,r'} T(\boldsymbol{l},\boldsymbol{r})\Big(\psi^\dagger(\boldsymbol{l})\psi(\boldsymbol{r}) - \psi^\dagger(\boldsymbol{r})\psi(\boldsymbol{l})\Big) \quad , \qquad \text{(A.5)}$$

so the current is:

$$\begin{aligned}
I &= \frac{ie}{\hbar}\sum_{l,r'} T(\boldsymbol{l},\boldsymbol{r})\left\langle\psi^\dagger(\boldsymbol{l})\psi(\boldsymbol{r}) - \psi^\dagger(\boldsymbol{r})\psi(\boldsymbol{l})\right\rangle \\
&= \frac{ie}{\hbar}\sum_{l,r'} T(\boldsymbol{l},\boldsymbol{r})\, 2i\Im\left\langle\psi^\dagger(\boldsymbol{l})\psi(\boldsymbol{r})\right\rangle \\
&= -\frac{2e}{\hbar}\sum_{l,r'} T(\boldsymbol{l},\boldsymbol{r})\,\Im\left\langle\psi^\dagger(\boldsymbol{l})\psi(\boldsymbol{r})\right\rangle \quad . \qquad \text{(A.6)}
\end{aligned}$$

We use the definition of the retarded Green's function at time $t = 0^+$

$$G^+(r,l,t) = -i\theta(t)\left\langle\left\{\psi(\boldsymbol{r},t), \psi^\dagger(\boldsymbol{l},0)\right\}\right\rangle \quad , \qquad \text{(A.7)}$$

$$G^K(\boldsymbol{r},\boldsymbol{l},t) = -i\left\langle\left[\psi(\boldsymbol{r},t), \psi^\dagger(\boldsymbol{l},0)\right]\right\rangle \quad , \qquad \text{(A.8)}$$

to represent the term in the current formula (A.6):

$$\left\langle\psi^\dagger(\boldsymbol{l},0)\psi\left(\boldsymbol{r},0^+\right)\right\rangle = \frac{i}{2}\left(G^+\left(r,l,0^+\right) - G^K\left(\boldsymbol{r},\boldsymbol{l},0^+\right)\right) \quad . \qquad \text{(A.9)}$$

Plugging this into the current (A.6) gives:

$$\begin{aligned} I &= -\frac{2e}{\hbar}\sum_{l,r'} T\left(\boldsymbol{l},\boldsymbol{r}\right)\Im\frac{i}{2}\left(G^{+}\left(r,l,0^{+}\right)-G^{K}\left(\boldsymbol{r},\boldsymbol{l},0^{+}\right)\right) \\ &= -\frac{e}{\hbar}\sum_{l,r'} T\left(\boldsymbol{l},\boldsymbol{r}\right)\Re\left(G^{+}\left(r,l,0^{+}\right)-G^{K}\left(\boldsymbol{r},\boldsymbol{l},0^{+}\right)\right) \\ &= \frac{e}{\hbar}\sum_{l,r'} T\left(\boldsymbol{l},\boldsymbol{r}\right)\Re\left(G^{K}\left(\boldsymbol{r},\boldsymbol{l},0^{+}\right)-G^{+}\left(r,l,0^{+}\right)\right) \end{aligned} \tag{A.10}$$

In order to simplify this expression [30] used the definition of Fourier transform at time $t=0^{+}$, $G\left(0^{+}\right)=\int\frac{d\omega}{2\pi}G\left(\omega\right)$, and obtained:

$$I=\frac{e}{\hbar}\int\frac{d\omega}{2\pi}\sum_{l,r'}T_{l,r}\Re\left(G_{r,l}^{K}\left(\omega\right)-G_{r,l}^{+}\left(\omega\right)\right)\ . \tag{A.11}$$

where the summation over r is a matrix product, and when combining the l sum it is precisely the definition a trace,

$$I=\frac{e}{\hbar}\int\frac{d\omega}{2\pi}TrT\Re\left(G^{K}\left(\omega\right)-G^{+}\left(\omega\right)\right)\ . \tag{A.12}$$

Further simplification was made using the spectral function $\rho(\epsilon)$ and its relation to $G^{+}(\omega)$:

$$\Re G^{+}\left(\omega\right)=P\int d\epsilon\frac{\rho\left(\epsilon\right)}{\omega-\epsilon}\ , \tag{A.13}$$

where the P before the integral represents the principal value of the integral. From (A.13) it is easy to see that

$$\int d\omega\Re G^{+}\left(\omega\right)=0\ , \tag{A.14}$$

plugging (A.14) into (A.12), we obtain the current expression:

$$I=\frac{e}{\hbar}\int\frac{d\omega}{2\pi}TrT\Re G^{K}\left(\omega\right)\ . \tag{A.15}$$

A.1.2 Evaluation of Keldysh Green's function

We started with the series:

$$G=G_{R}TG_{L}+G_{R}TG_{L}TG_{R}TG_{L}+...\ , \tag{A.16}$$

and summed the geometric seiries:

$$G=G_{R}TG_{L}\left(I-TG_{R}TG_{L}\right)^{-1}\ . \tag{A.17}$$

Preforming some matrix algebra yields:

$$G^{-1} = (I - TG_RTG_L)(G_RTG_L) - 1 \tag{A.18}$$
$$= (G_RTG_L)^{-1} - TG_RTG_L(G_RTG_L)^{-1} \tag{A.19}$$
$$= (G_RTG_L)^{-1} - T \ . \tag{A.20}$$

The Green's function operator we obtained in (A.1.2) can also be written as [38]:

$$G = \begin{pmatrix} G^+ & G^K \\ 0 & G^- \end{pmatrix} \ , \tag{A.21}$$

This relation enables us to extract G^K:

$$\begin{pmatrix} G^+ & G^K \\ 0 & G^- \end{pmatrix} = \left(\left(\begin{pmatrix} G_R^+ & G_R^K \\ 0 & G_R^- \end{pmatrix} \begin{pmatrix} T & 0 \\ 0 & T \end{pmatrix} \begin{pmatrix} G_L^+ & G_L^K \\ 0 & G_L^- \end{pmatrix} \right)^{-1} - \begin{pmatrix} T & 0 \\ 0 & T \end{pmatrix} \right)^{-1} . \tag{A.22}$$

Preforming some more matrix algebra:

$$\begin{pmatrix} G^+ & G^K \\ 0 & G^- \end{pmatrix} = \left(\begin{pmatrix} G_R^+TG_L^+ & G_R^+TG_L^K + G_R^KTG_L^- \\ 0 & G_R^-TG_L^- \end{pmatrix}^{-1} - \begin{pmatrix} T & 0 \\ 0 & T \end{pmatrix} \right)^{-1}$$
$$= \left(\begin{pmatrix} (G_R^+TG_L^+)^{-1} & -(G_R^+TG_L^+)^{-1}(G_R^+TG_L^K + G_R^KTG_L^-)(G_R^-TG_L^-)^{-1} \\ 0 & (G_R^-TG_L^-)^{-1} \end{pmatrix} - \begin{pmatrix} T & 0 \\ 0 & T \end{pmatrix} \right)^{-1} , \tag{A.23}$$

and calculating only the relevant term for G^K:

$$G^K = \left((G_R^+TG_L^+)^{-1} - T \right)^{-1} (G_R^+TG_L^+)^{-1} (G_R^+TG_L^K + G_R^KTG_L^-)(G_R^-TG_L^-)^{-1} \left((G_R^-TG_L^-)^{-1} - T \right)^{-1} \tag{A.24}$$

by using the double inversion:

$$\left(\left(\left((G_R^+TG_L^+)^{-1} - T \right)^{-1} (G_R^+TG_L^+)^{-1} \right)^{-1} \right)^{-1} = \left(\left((G_R^+TG_L^+)(G_R^+TG_L^+)^{-1} - (G_R^+TG_L^+)T \right) \right)^{-1}$$
$$= (I - G_R^+TG_L^+T)^{-1} \ ,$$

to simplify this expression

$$\left(\left((G_R^-TG_L^-)^{-1} \left((G_R^-TG_L^-)^{-1} - T \right)^{-1} \right)^{-1} \right)^{-1} = (I - TG_R^-TG_L^-)^{-1} \ ,$$

finally we obtain:

$$G^K = \left(I - G_R^+ T G_L^+ T\right)^{-1} \left(G_R^+ T G_L^K + G_R^K T G_L^-\right) \left(I - T G_R^- T G_L^-\right)^{-1} \ , \tag{A.25}$$

which expresses G^K only with the advanced and retarded Green's functions of the isolated parts of the Hamiltonian, using the relation $G_{L,R}^K = \left(1 - 2f_{L,R}\left(\omega\right)\right)\left(G_{L,R}^+ - G_{L,R}^-\right)$

$$\begin{aligned} G^K = \left(I - G_R^+ T G_L^+ T\right)^{-1} & \left[\left(1 - 2f_L\left(\omega\right)\right) G_R^+ T \left(G_L^+ - G_L^-\right)\right. \\ & \left. + \left(1 - 2f_R\left(\omega\right)\right)\left(G_R^+ - G_R^-\right) T G_L^-\right] \left(I - T G_R^- T G_L^-\right)^{-1} \ , \end{aligned} \tag{A.26}$$

this gives us the final expression for TG^K

$$\begin{aligned} TG^K = \left(I - T G_R^+ T G_L^+\right)^{-1} & \left[\left(1 - 2f_L\left(\omega\right)\right) T G_R^+ T \left(G_L^+ - G_L^-\right)\right. \\ & \left. + \left(1 - 2f_R\left(\omega\right)\right) T \left(G_R^+ - G_R^-\right) T G_L^-\right] \left(I - T G_R^- T G_L^-\right)^{-1} \ . \end{aligned} \tag{A.27}$$

A.2 Calculation of the tunneling matrix element

We demand continuity of the function and the derivative. At point a_1: $\psi_1\left(a_1\right) = \psi_2\left(a_1\right)$ gives:

$$A e^{i\kappa a_1} + B e^{-i\kappa a_1} = \frac{F}{\sqrt{\left|p\left(a_1\right)\right|}} + \frac{G}{\sqrt{\left|p\left(a_1\right)\right|}} \ , \tag{A.28}$$

and $\psi_1'\left(a_1\right) = \psi_2'\left(a_1\right)$:

$$A\left(i\kappa\right) e^{i\kappa a_1} + B\left(-i\kappa\right) e^{-i\kappa a_1} = \frac{F}{\sqrt{\left|p\left(a_1\right)\right|}} \frac{1}{\hbar} \left|p\left(a_1\right)\right| - \frac{G}{\sqrt{\left|p\left(a_1\right)\right|}} \frac{1}{\hbar} \left|p\left(a_1\right)\right| \ , \tag{A.29}$$

assuming $p'\left(x\right) \ll 1$, according to the WKB approximation. At point $a_1 + b$, the wave function: $\psi_2\left(b + a_1\right) = \psi_3\left(b + a_1\right)$ gives:

$$\frac{F}{\sqrt{\left|p\left(b + a_1\right)\right|}} e^{\tau} + \frac{G}{\sqrt{\left|p\left(b + a_1\right)\right|}} e^{-\tau} = C e^{ik\left(b + a_1\right)} \ , \tag{A.30}$$

and its derivative $\psi_2'\left(b + a_1\right) = \psi_3'\left(b + a_1\right)$:

$$\frac{F}{\sqrt{\left|p\left(b + a_1\right)\right|}} \frac{1}{\hbar} \left|p\left(b + a_1\right)\right| e^{\tau} - \frac{G}{\sqrt{\left|p\left(b + a_1\right)\right|}} \frac{1}{\hbar} \left|p\left(b + a_1\right)\right| e^{-\tau} = ikCe^{ikb} \ , \tag{A.31}$$

where $e^{\tau} \equiv e^{\frac{1}{\hbar}\int_{a_1}^{b+a_1} |p(x')| dx'}$.

Applying the boundary conditions, and preforming some algebra gives:

$$\frac{A}{C}=\frac{e^{ikb}e^{-i\kappa a}}{2i\kappa\sqrt{|p\left(a_1\right)|\left|p\left(b+a_1\right)\right|}}\left(\frac{1}{\hbar}\left|p\left(a_1\right)\right|+i\kappa\right)\left(\left|p\left(b+a_1\right)\right|\sinh\tau+ik\hbar\cosh\tau\right)\ \ , \tag{A.32}$$

so the absolute value square:

$$\left|\frac{A}{C}\right|^2=\frac{1}{4\kappa^2\left|p\left(a_1\right)\right|\left|p\left(b+a_1\right)\right|}\left(\frac{1}{\hbar}^2\left|p\left(a_1\right)\right|^2+\kappa^2\right)\left(\left|p\left(b+a_1\right)\right|^2\sinh^2\tau+k^2\hbar^2\cosh^2\tau\right). \tag{A.33}$$

Plugging the momenta and applying all the assumptions as written in (2.3.2) we obtain:

$$\left|\frac{A}{C}\right|^2=\frac{V_a-V_0}{4\left(E-V_0\right)}\sinh^2\tau\ \ , \tag{A.34}$$

which leads to the probability to overcome the potential barrier:

$$P_{pass}=\left|\frac{C}{A}\right|^2=\frac{16\left(E-V_0\right)}{\left(V_a-V_0\right)}e^{-2\tau}\ \ . \tag{A.35}$$

A.3 Relation between local density of states and Green's function

We would like to show a simple proof of the relation between the imaginary part of the Green's function to the local density of states:

$$N\left(r_0,E\right)=-\frac{1}{\pi}ImG^+\left(r_0,r_0,E\right) \tag{A.36}$$

Let us begin with the spectral decomposition of the advanced Green function:

$$\lim_{\epsilon\to0}\frac{1}{E-E_i+i\epsilon}=PP\left(\frac{1}{E-E_i}\right)-i\pi\delta\left(E-E_i\right)\ \ , \tag{A.37}$$

and use the theorem:

$$\lim_{\epsilon\to0}\frac{1}{E-E_i+i\epsilon}=PP\left(\frac{1}{E-E_i}\right)-i\pi\delta\left(E-E_i\right)\ \ , \tag{A.38}$$

where PP is the principle part. Taking the imaginary part of the spectral decomposition:

$$ImG^+\left(r,r,E\right)=\sum_i Im\left(PP\left(\frac{1}{E-E_i}\right)-i\pi\delta\left(E-E_i\right)\right)\left|\psi_i\left(r\right)\right|^2 \tag{A.39}$$

$$=-\pi\sum_i\delta\left(E-E_i\right)\left|\psi_i\left(r\right)\right|^2\ \ , \tag{A.40}$$

and reorganising the equation, gives the exact definition of the local density of states:

$$-\frac{1}{\pi}ImG^{+}\left(r,r,E\right)=\sum_{i}\delta\left(E-E_{i}\right)\left|\psi_{i}\left(r\right)\right|^{2}\equiv N\left(r,E\right)\ . \tag{A.41}$$

A.4 Dirac Hamiltonian with scalar field interactions

In order to connect the Hamiltonian:

$$\Psi^{*}\left(r\right)K\Psi\left(r\right)=\Psi^{*}\left(r\right)\left(\begin{array}{cc}\boldsymbol{\sigma}\cdot\boldsymbol{p} & \Delta\left(\boldsymbol{r}\right)\\ \Delta^{*}\left(\boldsymbol{r}\right) & -\boldsymbol{\sigma}\cdot\boldsymbol{p}\end{array}\right)\Psi\left(r\right) \tag{A.42}$$

to the one we used (3.13), we will change this expression using the definition: $\Delta\left(\boldsymbol{r}\right)=g\varphi\left(\boldsymbol{r}\right)=g\left(\varphi_{1}+i\varphi_{2}\right)$:

$$\begin{aligned}\Psi^{*}\left(r\right)K\Psi\left(r\right)&=\Psi^{*}\left(r\right)\left[\left(\begin{array}{cc}\boldsymbol{\sigma}\cdot\boldsymbol{p} & 0\\ 0 & -\boldsymbol{\sigma}\cdot\boldsymbol{p}\end{array}\right)+g\left(\begin{array}{cc}0 & \varphi_{1}+i\varphi_{2}\\ \varphi_{1}-i\varphi_{2} & 0\end{array}\right)\right]\Psi\left(r\right)\\&=\Psi^{*}\left(r\right)\left[\left(\begin{array}{cc}\boldsymbol{\sigma}\cdot\boldsymbol{p} & 0\\ 0 & -\boldsymbol{\sigma}\cdot\boldsymbol{p}\end{array}\right)+g\left[\varphi_{1}\left(\begin{array}{cc}0 & I\\ I & 0\end{array}\right)-i\varphi_{2}\left(\begin{array}{cc}0 & -I\\ I & 0\end{array}\right)\right]\right]\Psi\left(r\right)\\&=\Psi^{*}\left(r\right)\left[\left(\begin{array}{cc}\boldsymbol{\sigma}\cdot\boldsymbol{p} & 0\\ 0 & -\boldsymbol{\sigma}\cdot\boldsymbol{p}\end{array}\right)+g\left(\begin{array}{cc}0 & I\\ I & 0\end{array}\right)\left[\varphi_{1}-i\varphi_{2}\left(\begin{array}{cc}I & 0\\ 0 & -I\end{array}\right)\right]\right]\Psi\left(r\right)\end{aligned} \tag{A.43}$$

now we can express each of the remaining matrices:

$$\boldsymbol{\alpha}=\left(\begin{array}{cc}\boldsymbol{\sigma} & 0\\ 0 & -\boldsymbol{\sigma}\end{array}\right),\ \beta=\left(\begin{array}{cc}0 & I\\ I & 0\end{array}\right),\ \gamma_{5}=-i\alpha^{1}\alpha^{2}\alpha^{3}=\left(\begin{array}{cc}I & 0\\ 0 & -I\end{array}\right)\ ,$$

and obtain:

$$\Psi^{*}\left(r\right)K\Psi\left(r\right)=\Psi^{*}\left(r\right)\left(\boldsymbol{\alpha}\cdot\boldsymbol{p}+g\beta\left(\varphi_{1}-i\varphi_{2}\gamma_{5}\right)\right)\Psi\left(r\right)\ . \tag{A.44}$$

The interaction term when: $\varphi=\varphi_{1}+i\varphi_{2}=\left|\varphi\right|e^{i\chi}$, $\varphi_{1}=\Re\left|\varphi\right|e^{i\chi}=\left|\varphi\right|\cos\chi$, $\varphi_{2}=\Im\left|\varphi\right|e^{i\chi}=\left|\varphi\right|\sin\chi$, can be written as:

$$\begin{aligned}\left|\varphi\right|\Psi^{*}\beta e^{-i\gamma_{5}\chi}\Psi&=\left|\varphi\right|\Psi^{*}\beta\left(1-i\gamma_{5}\chi+\frac{1}{2!}\left(-i\gamma_{5}\chi\right)^{2}+\frac{1}{3!}\left(-i\gamma_{5}\chi\right)^{3}+...\right)\Psi\\&=\left|\varphi\right|\Psi^{*}\beta\left(1-i\gamma_{5}\chi-\frac{1}{2!}\chi^{2}+i\frac{1}{3!}\gamma_{5}\chi^{3}+\frac{1}{4!}\chi^{4}+...\right)\Psi\\&=\left|\varphi\right|\Psi^{*}\beta\left(1-\frac{1}{2!}\chi^{2}+\frac{1}{4!}\chi^{4}-i\gamma_{5}\left(\chi-\frac{1}{3!}\chi^{3}\right)+...\right)\Psi\\&=\left|\varphi\right|\Psi^{*}\beta\left(\cos\chi-i\gamma_{5}\sin\chi\right)\Psi\\&=\Psi^{*}\beta\left(\varphi_{1}-i\gamma_{5}\varphi_{2}\right)\Psi\end{aligned} \tag{A.45}$$

such that preforming a chiral gauge transformation to this term keeps it invariant:

$$\begin{aligned} H'_{int} &= \Psi^* e^{-i\omega\gamma_5} \left(g \left|\varphi\right| \beta e^{-i\gamma_5(\chi+2\omega)} \right) e^{i\omega\gamma_5} \Psi \\ &= \Psi^* e^{-i\omega\gamma_5} \left(g \left|\varphi\right| \beta e^{-i\gamma_5\chi} e^{-i\omega\gamma_5} \right) \Psi \\ &= \Psi^* e^{-i\omega\gamma_5} \left(g \left|\varphi\right| e^{i\omega\gamma_5} \beta e^{-i\gamma_5\chi} \right) \Psi \\ &= \Psi^* \left(g \left|\varphi\right| \beta e^{-i\gamma_5\chi} \right) \Psi = H_{int} \end{aligned} \tag{A.46}$$

In order to keep this axial symmetry, when coupling to a gauge field, the same symmetry is used.

References

[1] K. S. Novoselov, A. K. Geim, S. V. Morozov, D. Jiang, Y. Zhang, S. V. Dubonos, I. V. Grigorieva, and A. A. Firsov, "Electric field effect in atomically thin carbon films", Science **306**, 666–669 (2004).

[2] A. H. Castro Neto, F. Guinea, N. M. R. Peres, K. S. Novoselov, and A. K. Geim, "The electronic properties of graphene", Rev. Mod. Phys. **81**, 109–162 (2009).

[3] L. A. Falkovsky, "Optical properties of graphene", Journal of Physics: Conference Series **129**, 012004 (2008).

[4] R. R. Nair, P. Blake, A. N. Grigorenko, K. S. Novoselov, T. J. Booth, T. Stauber, N. M. R. Peres, and A. K. Geim, "Fine structure constant defines visual transparency of graphene", Science **320**, 1308–1308 (2008).

[5] C. Lee, X. Wei, J. W. Kysar, and J. Hone, "Measurement of the elastic properties and intrinsic strength of monolayer graphene", Science **321**, 385–388 (2008).

[6] A. A. Balandin, S. Ghosh, W. Bao, I. Calizo, D. Teweldebrhan, F. Miao, and C. N. Lau, "Superior thermal conductivity of single-layer graphene", Nano Letters **8**, PMID: 18284217, 902–907 (2008).

[7] G. W. Semenoff, "Condensed-matter simulation of a three-dimensional anomaly", Phys. Rev. Lett. **53**, 2449–2452 (1984).

[8] A. V. Shytov, M. I. Katsnelson, and L. S. Levitov, "Atomic collapse and quasi–Rydberg states in graphene", Phys. Rev. Lett. **99**, 246802 (2007).

[9] V. M. Pereira, J. Nilsson, and A. H. Castro Neto, "Coulomb impurity problem in graphene", Phys. Rev. Lett. **99**, 166802 (2007).

[10] M. M. Fogler, D. S. Novikov, and B. I. Shklovskii, "Screening of a hypercritical charge in graphene", Phys. Rev. B **76**, 233402 (2007).

[11] J.-H. Chen, L. Li, W. G. Cullen, and M. S. Fuhrer, "Tunable Kondo effect in graphene with defects", Nature Physics **7**, 535–538 (2011).

[12] M. M. Ugeda, I. Brihuega, F. Guinea, and J. M. Gómez-Rodríguez, "Missing atom as a source of carbon magnetism", Phys. Rev. Lett. **104**, 096804 (2010).

[13] Y. Liu, M. Weinert, and L. Li, "Determining charge state of graphene vacancy by noncontact atomic force microscopy and first-principles calculations.", Nanotechnology **26** (2015).

[14] J. Mao, Y. Jiang, D. Moldovan, G. Li, K. Watanabe, T. Taniguchi, M. R. Masir, F. M. Peeters, and E. Y. Andrei, "Realization of a tunable artificial atom at a supercritically charged vacancy in graphene", Nature Physics **12**, 545–549 (2016).

[15] O. Ovdat, J. Mao, Y. Jiang, E. Y. Andrei, and E. Akkermans, "Observing a scale anomaly and a universal quantum phase transition in graphene", Nature Communications **8** (2017).

[16] O. Ovdat, Y. Don, and E. Akkermans, "Vacancies in graphene: Dirac physics and fractional vacuum charges", Phys. Rev. B **102**, 075109 (2020).

[17] P. R. Wallace, "The band theory of graphite", Phys. Rev. **71**, 622–634 (1947).

[18] S. Reich, J. Maultzsch, C. Thomsen, and P. Ordejón, "Tight-binding description of graphene", Phys. Rev. B **66**, 035412 (2002).

[19] M. I. Katsnelson, *Graphene carbon in two dimensions* (Cambridge university press, 1979).

[20] C. A. Coulson and G. S. Rushbrooke, "Note on the method of molecular orbitals", Mathematical Proceedings of the Cambridge Philosophical Society **36**, 193–200 (1940).

[21] M. Rigby and R. Mallion, "On the eigenvalues and eigenvectors of certain finite, vertex-weighted, bipartite graphs", Journal of Combinatorial Theory, Series B **27**, 122–129 (1979).

[22] O. Lehtinen, J. Kotakoski, A. V. Krasheninnikov, A. Tolvanen, K. Nordlund, and J. Keinonen, "Effects of ion bombardment on a two-dimensional target: atomistic simulations of graphene irradiation", Phys. Rev. B **81**, 153401 (2010).

[23] V. M. Pereira, F. Guinea, J. M. B. Lopes dos Santos, N. M. R. Peres, and A. H. Castro Neto, "Disorder induced localized states in graphene", Phys. Rev. Lett. **96**, 036801 (2006).

[24] Y. Nishida, "Vacuum polarization of graphene with a supercritical Coulomb impurity: low-energy universality and discrete scale invariance", Phys. Rev. B **90**, 165414 (2014).

[25] V. M. Pereira, J. M. B. Lopes dos Santos, and A. H. Castro Neto, "Modeling disorder in graphene", Phys. Rev. B **77**, 115109 (2008).

[26] G. Binnig, H. Rohrer, C. Gerber, and E. Weibel, "Surface studies by scanning tunneling microscopy", Phys. Rev. Lett. **49**, 57–61 (1982).

[27] G. Binnig and H. Rohrer, "Scanning tunneling microscopy", Surface Science **126**, 236–244 (1983).

[28] A. Vázquez De Parga and R. Miranda, "6 – Scanning tunneling microscopy (STM) of graphene", in *Graphene*, edited by V. Skákalová and A. B. Kaiser (Woodhead Publishing, 2014), pp. 124–155.

[29] Ø. Fischer, M. Kugler, I. Maggio-Aprile, C. Berthod, and C. Renner, "Scanning tunneling spectroscopy of high-temperature superconductors", Rev. Mod. Phys. **79**, 353–419 (2007).

[30] C. Berthod and T. Giamarchi, "Tunneling conductance and local density of states in tight-binding junctions", Phys. Rev. B **84**, 155414 (2011).

[31] R. E. Prange, "Tunneling from a many-particle point of view", Phys. Rev. **131**, 1083–1086 (1963).

[32] A. Messiah, *Quantum mechanics* (Dover Publications, 1999).

[33] W. A. Harrison, *Solid state theory* (Dover Publications, 1979).

[34] C. Chamon, C.-Y. Hou, R. Jackiw, C. Mudry, S.-Y. Pi, and G. Semenoff, "Electron fractionalization for two-dimensional Dirac fermions", Phys. Rev. B **77**, 235431 (2008).

[35] R. Jackiw and S.-Y. Pi, "Chiral gauge theory for graphene", Phys. Rev. Lett. **98**, 266402 (2007).

[36] H. Hammar, P. Berggren, and J. Fransson, "Molecular graphene under the eye of scattering theory", Physical Review B **88** (2013).

[37] C.-Y. Hou, C. Chamon, and C. Mudry, "Electron fractionalization in two-dimensional graphenelike structures", Physical Review Letters **98** (2007).

[38] J. Rammer and H. Smith, "Quantum field-theoretical methods in transport theory of metals", Rev. Mod. Phys. **58**, 323–359 (1986).

ההסתברות לא יכולה לחדור את גבולותיו. כתוצאה מדרישה זאת, נוצר אילוץ אשר מוביל לבחירת תנאי שפה מיוחדים הנקראים "קיראלים". תיאור זה של הבעיה, באמצעות תנאי שפה קיראלים, מצליח להסביר את כל התופעות שנצפו בגרפן עם חוסר באטום, פרט להיסט במצבי האנרגיה שנוספו.

מטרתנו הראשית היא להסביר את הזזת מצבי האנרגיה הנ"ל, על ידי אינטראקציה בין רקמת הגרפן לבין מכשיר המדידה (מיקרוסקופ מינהור סורק) TUNNELING MICROSCOPY SCANNING (STM). ישנן שתי סיבות עיקריות בגינן מערכת המדידה יכולה להיות הגורם להזזה. ראשית, מערכת מדידה זאת מבוססת על מנהור של אלקטרונים בין קצה הטיפ באמצעותו מודדים לבין רקמת הגרפן. מנהור זה יוצר זרם אלקטרונים שנמדד במעבדה, וגודלו מוכרח להיות מסדר גודל הניתן למדידה. לכן, האינטראקציה שנוצרת בין גרפן למערכת המדידה היא מסדר הגודל של האות הנמדד ולא ניתן להזניחה. שנית, אין כל סיבה שמערכת המדידה ואיבר האינטראקציה יהיו בעלי ספקטרום אנרגיה סימטרי. לכן, ניתן להסביר את תזוזת מצבי האנרגיה בעזרת איבר האינטראקציה הנובע ממנהור, כפי שניתן לראות בתוצאות.

לאחר מכן, בשלב ניתוח התוצאות, נרצה לעמוד על ההבדלים בין שני ביטויים למוליכות חשמלית הנובעת ממנהור. הביטוי הראשון, המוכר מספרי הלימוד, מבוסס על קירוב של מינהור ישיר (סדר ראשון בתורה ההפרעות אשר מסתמך על חוק הזהב של פרמי). מנגד, הביטוי השני מורכב בהרבה היות והוא לוקח בחשבון את כל מסלולי המנהור האפשריים בין רקמת הגרפן עם חוסר באטום ומערכת המדידה. השאלה הראשית בה נרצה לדון בניתוח זה היא האם השימוש שלנו בביטוי המורכב נחוץ להסברת היסט מוד האנרגיה או שניתן להסביר את התופעה בעזרת הביטוי הפשוט יותר. מעבר לניתוח זה, נרצה גם לבדוק הנחה רווחת אשר סוברת כי התלות של מכשיר המדידה באנרגיה קטנה וניתנת להזנחה ביחס לדגימה אותה מודדים.

לבסוף, נרצה להציע דרך להסברת תופעה אשר התגלתה בניסוי, בו המצב היציב של המטען שנצבר סביב גבולות האטום החסר השתנה. מהלך הניסוי, אשר גרם לשינוי במטען, כלל יישום הלם בעל מתח גבוה בעזרת קצה מכשיר המדידה (הממוקם בדיוק מעל האטום החסר). מבחינה תאורתית, הלם זה מתואר על ידי תלות זמנית של הפוטנציאל בבעיה. יתר על כן, השילוב בין תנאי השפה המורכבים ("קיראלים") שמתארים גרפן עם אטום חסר לבין פוטנציאל תלוי זמן זה, הופכים את הבעיה למורכבת מאוד לפתירה. אנו מציעים דרך לפשט את הבעיה באמצעות מודל מתמטי המכיל תכונות פיזיקאליות דומות מאוד לאלו שנצפו בגרפן חסר אטום. במודל המוצע, ישנה אינטראקציה בין פרמיוני דיראק המתארים גרפן לבין שדה כיול, אך שתי הבעיות לא מכילות את אותן הסימטריות ולכן לא יכולות להיות זהות פיזיקאלית. כתוצאה מכך, בשלב הסופי של עבודתנו נעמוד על ההבדלים בין שני המודלים ונסביר בדיוק מהו המקור לשוני בין הסימטריות ומה ניתן לעשות על מנת להסירו.

תקציר

גרפן, החומר הדו־מימדי הראשון שיוצר באופן יציב, מורכב מרקמה משושה בודדת של אטומי פחמן. בעקבות הפקתו במעבדה ובדיקת תכונותיו, מגוון רחב של מאפיינים ייחודיים התגלו ועל כן כיום הוא מהווה בסיס למחקר בתחומים רבים. החל ממאפייניו האופטיים, המכאניים, הכימיים וההנדסיים ועד לסגולותיו האלקטרוניות בהן בין היתר נתמקד בעבודה זאת. למרות גילויו בשנת 2004, שנים רבות לפני כן נוצר מודל אשר מנתח שכבה יחידה של גרפית על ידי הצגת הרקמה המשושה בעזרת שתי רקמות משולשות אשר שזורות יחדיו. פתרון מודל זה המסתמך על מודל השזירה האדוקה מניב את ספקטרום האנרגיה של גרפן ומהווה בסיס למציאת תכונות אלקטרוניות רבות.

לרוב, בחומרים קריסטליים כדוגמת גרפן, בעלי רקמת אטומים מסודרת, היחס לליקויים בגביש כגון מזהמים וחוסרים באטומים, הוא כאל הפרעות המופיעות בטבע למורת רוחם של החוקרים. למרות דעה רווחת זאת, חוסרים של אטומים בגרפן מובילים לסממנים פיזיקאלים שלא הופיעו כאשר הרקמה הייתה ללא חורים, כגון: הצטברות של מטען באזור קצוות החור הנוצר, שבירה של סימטריה לשיקוף הרקמה תוך החלפת שתי תתי הרקמות, (אשר נשמרה עבור רקמת גרפן) והוספה של מצבים (מודים עם אנרגית פרמי) לספקטרום האנרגיה של גרפן.

גרפן, ללא חוסר באטומים, ניחן בספקטרום אנרגיה סימטרי סביב אנרגית פרמי. יתר על כן, על פי התאוריה הסרת אטום מהרקמה הורסת את הקשרים הסובבים את האטום שהוסר. לכן, פעולה זאת לא מוסיפה גודל אנרגטי לרקמה, כך שהסימטריה של מצבי האנרגיה צריכה להישמר. בעקבות זאת, התאוריה גורסת כי מצבי האנרגיה שנוספו כתוצאה מהסרת האטום ממוקמים בדיוק באנרגית פרמי (כך שהסימטריה נשמרת). אך, בניגוד למודל התאורתי, מדידות מראות סטיה עיקבית של מצבים אלו מאנרגית פרמי. לכן, ישנו גורם נוסף אשר שובר את סימטריית ספקטרום האנרגיה ומוביל להזזת המצבים שנוספו אשר לא נלקח בחשבון עד כה.

מבחינה תיאורתית, ישנן שתי דרכים למדל את הבעיה של גרפן חסר אטומים. מודל ראשון מוסיף איבר של פוטנציאל קולון להמילטוניאן האפקטיבי של גרפן, אך מודל זה לוקה בחסר בין היתר היות והוא לא מסוגל לחזות את המטען הנצבר בשפת החור. לחילופין, המודל השני מתייחס לחור ברקמת הגרפן כאל מפזר מושלם, כך שצפיפות

המחקר בוצע בהנחייתו של פרופסור אריק אקרמן בפקולטה לפיזיקה.

תודות

אני רוצה להודות למנחה שלי פרופ. אריק אקרמן על התמיכה אני רוצה להודות למנחה שלי פרופ. אריק אקרמן על התמיכה והעזרה במהלך כל התואר ובמיוחד בזמן כתיבת עבודה זאת. כל שיחת התייעצות איתך הייתה מפרה ומלמדת, מצד אחד עזרת לי לארגן את הרעיונות שלי ולהבין כיצד לגשת לפתרון בעיות ומצד שני במהלך השיחות הערותיך הובילו למחשבות וכיוונים חדשים למחקר, על כך אני אסירת תודה.

תודה מיוחדת להורי ומשפחתי על התמיכה וההשראה שנתנו לי במהלך כל חיי.

אני מודה לטכניון על התמיכה הכספית הנדיבה בהשתלמותי.

השפעת מדידות STM על גרפן נטול אטומים

חיבור על מחקר

לשם מילוי חלקי של הדרישות לקבלת התואר
מגיסטר למדעים בפיזיקה

יובל אבולעפיה

הוגש לסנט הטכניון --- מכון טכנולוגי לישראל
תישרי התשפ"א חיפה ספטמבר 2020

השפעת מדידות STM על גרפן נטול אטומים

יובל אבולעפיה